ELSEVIER

International Journal of Solids and Structures 41 (2004) 4661–4684

INTERNATIONAL JOURNAL OF SOLIDS and STRUCTURES

www.elsevier.com/locate/ijsolstr

An efficient higher order zigzag theory for laminated plates subjected to thermal loading

S. Kapuria [a,*], G.G.S. Achary [b]

[a] *Applied Mechanics Department, IIT Delhi, Hauz Khas, New Delhi 110016, India*
[b] *ETD Department, Engineers India Limited, Bhikaji Cama Place, New Delhi 110066, India*

Received 23 July 2003; received in revised form 11 February 2004
Available online 17 April 2004

Abstract

A new efficient higher order zigzag theory is presented for laminated plates under thermal loading. The third order zigzag model is modified by replacing the uniform across the thickness approximation for the deflection with a layer-wise variable approximation for deflection which explicitly accounts for the transverse thermal strain. The thermal field is approximated as piecewise linear across the sub-layers. The displacement field is expressed in terms of the thermal field and only five primary displacement variables by satisfying exactly the conditions of zero transverse shear stresses at the top and the bottom and their continuity at the layer interfaces. The governing equations are derived using the principle of virtual work. Comparison of Navier solutions for simply-supported rectangular test plate devised for this study and composite and sandwich plates with the exact three-dimensional thermo-elasticity solutions for two kinds of thermal loads establishes that the present efficient zigzag theory is generally more accurate than the existing zigzag theory.

Keywords: Zigzag theory; Thermal load; Composite plate; Sandwich plate; Exact solution

1. Introduction

The composite and sandwich structural components used in aerospace, underwater and land based structures are often subjected to moderate to severe environment or process based thermal loading causing significant thermal stresses due to thermal gradient across the thickness and due to widely different thermal properties of the adjacent laminas. These laminated components have excellent strength to weight and stiffness to weight ratio, but relatively poor strength and stiffness for transverse shear. Hence transverse shear plays a significant role for the moderately thick and thick laminated structures. Moreover, the layer-wise material inhomogeneity causes a severe layer-wise distortion of the normal to the mid-surface and it also gets strained primarily due to the thermal strain. The equivalent single layer (ESL) theories like the

* Corresponding author. Tel.: +91-112-659-1218; fax: +91-112-658-1119.
E-mail address: kapuria@am.iitd.ac.in (S. Kapuria).

0020-7683/$ - see front matter © 2004 Elsevier Ltd. All rights reserved.
doi:10.1016/j.ijsolstr.2004.02.020

classical laminate theory (CLT), first order shear deformation theory (FSDT), the third order theories (TOTs) and higher order theories (HOTs) are inadequate to account for this distortion and violate the shear stress continuity conditions at the layer interfaces. Tauchert (1991), Noor and Burton (1992), Murakami (1993), Reddy (1997), Argyris and Tanek (1997) and Carrera (2000) have reviewed plate theories for thermo-mechanical response. CLT, FSDT and TOTs have been applied to thermal stress analysis of laminated plates (e.g., Stavsky, 1963; Nemrovskii, 1972; Wu and Tauchert, 1980a,b; Reddy and Hsu, 1980; Kheider and Reddy, 1991; He, 1995; Locke, 1997). HOTs for thermal loading of laminated plates have been developed by Jonnalagadda et al. (1993), Kant and Khare (1994), Rohwer et al. (2001) and Patel et al. (2002). Rohwer et al. (2001) demonstrated that the transverse shear and normal stress components can be predicted with good accuracy from HOTs using the 3D equilibrium equations for cross-ply layered plates under assumed linear temperature variation across the thickness.

Finite element analysis based on 3D elasticity equations and quasi-3D finite element analysis based on discrete layer theories (DLTs) for plates with layer-wise expansions of displacements are more accurate than the ESL theories, but are computationally expensive for real structural analysis since the number of displacement variables depend on the number of layers. To overcome this, zigzag theories have been developed for composite laminates in which the slope discontinuity in the in-plane displacements at the layer interfaces is introduced through a zigzag function with values of +1 and −1 at successive layer interfaces (Ali et al., 1999). More consistent efficient zigzag theories have been developed with layer-wise expansion of displacements in which the number of primary displacement unknowns is reduced to those of the ESL theory of the same order, by imposing the conditions on the continuity of transverse shear stresses at the layer interfaces and by also possibly imposing the shear traction-free conditions at the top and the bottom surfaces. Xioping and Liangxin (1994) developed an efficient third order zigzag model for plates under thermal loading. Rolfes et al. (1998), Noor and Malik (1999, 2000) and Park and Kim (2002) have presented various two-step or multi-step predictor–corrector procedures for plates under thermal loading. Carrera (2002) has presented a variety of displacement-based ESL theories and discrete layer theories, and also mixed stress and displacement-based discrete layer theories for thermal stress analysis of plates and assessed them for assumed linear temperature profile across the thickness and an actual temperature profile based on the heat conduction equation. It was concluded that: (1) the ESLs yield inaccurate results even for thin plates; (2) the advanced zigzag theories may work well in thick plates loaded by assumed linear temperature profile but yield inaccurate results for actual temperature profile based on the heat conduction equation; (3) at least a quadratic layer-wise variation of deflection w with z is required to capture even the linear thermal strain in the thickness direction. Exact thermo-elasticity solutions (Tungikar and Rao, 1994) reveal that the non-uniformity in the deflection across the thickness, primarily due to the thermal strain, has enormous bearing on the results. Except for the DLTs in which layer-wise expansion is taken for w, no other available theory includes the transverse thermal strain. Kapuria et al. (2003) have recently presented an accurate and efficient higher order zigzag theory for thermal stress analysis of laminated beams using a variable approximation for deflection across the thickness which, for the first time, explicitly accounts for the transverse thermal strain.

An efficient 2D higher order zigzag theory is developed in this work for thermal stress analysis of composite and sandwich plates, in line with the higher order zigzag theory of Kapuria et al. (2003) for beams, with modification of the existing zigzag thermal model (Xioping and Liangxin, 1994) for plates by choosing an approximation of the transverse displacement w which accounts for the transverse thermal strain due to thermal expansion coefficient α_3. The axial displacements are approximated as a combination of a global third order variation across the thickness with an additional layer-wise linear variation. The thermal field is approximated sub-layer-wise as piecewise linear. The displacement field is expressed in terms of only five primary displacement variables and the thermal field by satisfying exactly the conditions of zero transverse shear stresses at the top and the bottom surface of the plate and their continuity at the layer interfaces. The equilibrium equations and the boundary conditions are derived using the principle of virtual

work. This theory is computationally efficient as the number of primary displacement unknowns is the same as in the FSDT. Analytical Fourier series solutions are obtained for the response of simply-supported plates under thermal loads. The existing zigzag theory (ZIGT) of Xioping and Liangxin (1994) for plates is obtained as a particular case of the present theory by setting $\alpha_3 = 0$ for all the layers. The present higher order zigzag theory (HZIGT) is assessed by comparison with the exact 3D thermo-elasticity, the existing zigzag theory (ZIGT) and the FSDT solutions. Numerical results for the displacements and the stresses for a benchmark test plate devised for this study, composite symmetric and anti-symmetric cross-ply laminated plates and sandwich plates establish that the present HZIGT is much superior to the FSDT and ZIGT.

2. Approximation of displacement fields

Consider a cross-ply composite or sandwich plate (Fig. 1) made of L perfectly bonded orthotropic plies of total thickness h with the mid-plane chosen as the xy-plane with $z = z_0 = -h/2$ as the bottom surface and $z = z_L = h/2$ as the top surface. The kth ply from the bottom has bottom surface at $z = z_{k-1}$. The reference plane $z = 0$ either passes through or is the bottom surface of the k_0th layer. Let $u_x, u_y; w$ be the in-plane and transverse displacements. Denoting differentiation by a subscript comma, the strain–displacement relations are:

$$\varepsilon_x = u_{x,x}, \quad \varepsilon_y = u_{y,y}, \quad \varepsilon_z = w_{,z}, \quad \gamma_{xy} = u_{x,y} + u_{y,x}, \quad \gamma_{yz} = u_{y,z} + w_{,y}, \quad \gamma_{zx} = u_{x,z} + w_{,x}. \tag{1}$$

For the temperature rise θ, assuming transverse normal stress $\sigma_z \simeq 0$, the linear constitutive equations for the stresses σ, τ are expressed as

$$\sigma = \overline{Q}\varepsilon - \bar{\beta}\theta, \quad \tau = \widehat{Q}\gamma, \tag{2}$$

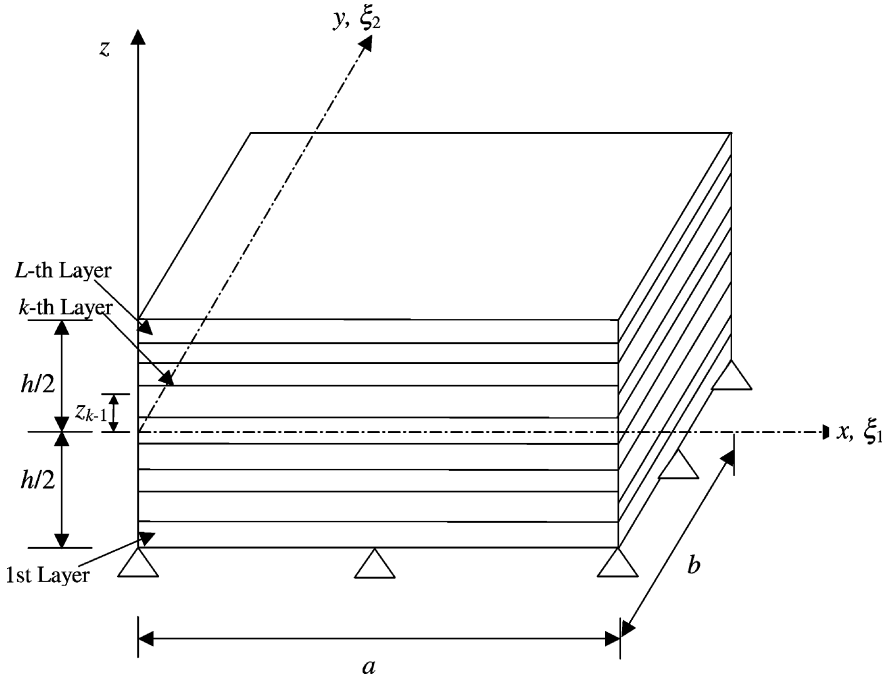

Fig. 1. Geometry of a laminated plate.

where

$$\sigma = \begin{bmatrix} \sigma_x \\ \sigma_y \\ \tau_{xy} \end{bmatrix}, \quad \tau = \begin{bmatrix} \tau_{zx} \\ \tau_{yz} \end{bmatrix}, \quad \varepsilon = \begin{bmatrix} \varepsilon_x \\ \varepsilon_y \\ \gamma_{xy} \end{bmatrix}, \quad \gamma = \begin{bmatrix} \gamma_{zx} \\ \gamma_{yz} \end{bmatrix}, \tag{3}$$

$$\overline{Q} = \begin{bmatrix} \overline{Q}_{11} & \overline{Q}_{12} & 0 \\ \overline{Q}_{12} & \overline{Q}_{22} & 0 \\ 0 & 0 & \overline{Q}_{66} \end{bmatrix}, \quad \widehat{Q} = \begin{bmatrix} \overline{Q}_{55} & 0 \\ 0 & \overline{Q}_{44} \end{bmatrix}, \quad \bar{\beta} = \begin{bmatrix} \bar{\beta}_1 \\ \bar{\beta}_2 \\ 0 \end{bmatrix}, \tag{4}$$

where $\overline{Q}_{ij}$ are the reduced elastic stiffness and $\bar{\beta}_i$ are the stress–temperature coefficients.

The temperature field $\theta(x, y, z)$ for the plate can be solved analytically for some geometries or by the finite element method. For the 2D model developed herein, θ is approximated as piecewise linear across the thickness, in terms of its values at n_θ points at $z_\theta^l, l = 1, 2, \ldots, n_\theta$ with $z_\theta^1 = z_0, z_\theta^{n_\theta} = z_L$:

$$\theta(x, y, z) = \Psi_\theta^l(z)\theta^l(x, y), \tag{5}$$

where $\theta^l(x, y) = \theta(x, y, z_\theta^l)$. $\Psi_\theta^l(z)$ are linear interpolation functions and summation convention is used for the index l. n_θ can differ from L with $n_\theta \geqslant L$. Each layer is divided into sub-layers for discretisation of θ whose number is determined by the required accuracy. The functional form of $\theta^l(x, y)$ will depend on the boundary conditions.

Three-dimensional thermo-elasticity exact solutions (Tungikar and Rao, 1994) reveal that for moderately thick plates under thermal load, the deflection w has significant variation across the thickness due to the much greater thermal contribution to ε_z compared to the negligible contribution of the stresses $\sigma_x, \sigma_y, \sigma_z$. Hence, herein w is approximated by integrating the constitutive equation for ε_z by including only the thermal contribution

$$w(x, y, z) = w_0(x, y) + \overline{\Psi}_\theta^l(z)\theta^l(x, y), \tag{6}$$

where $\overline{\Psi}_\theta^l(z) = \int_0^z \alpha_3 \Psi_\theta^l(z)\,\mathrm{d}z$ is a piecewise quadratic function. For the kth layer, u_x, u_y are approximated across the thickness as a combination of a third-order variation in z and a layer-wise linear variation:

$$u(x, y, z) = u_k(x, y) - z w_{0_d}(x, y) + z\psi_k(x, y) + z^2\xi(x, y) + z^3\eta(x, y), \tag{7}$$

$$u = \begin{bmatrix} u_x \\ u_y \end{bmatrix}, \quad w_{0_d} = \begin{bmatrix} w_{0,x} \\ w_{0,y} \end{bmatrix}, \quad u_k = \begin{bmatrix} u_{k_x} \\ u_{k_y} \end{bmatrix}, \quad \psi_k = \begin{bmatrix} \psi_{k_x} \\ \psi_{k_y} \end{bmatrix}, \quad \xi = \begin{bmatrix} \xi_x \\ \xi_y \end{bmatrix}, \quad \eta = \begin{bmatrix} \eta_x \\ \eta_y \end{bmatrix}. \tag{8}$$

u_k and ψ_k denote the translation and rotation variables of the kth layer.

Substituting u_x, u_y, w from Eqs. (7) and (6), and θ from Eq. (5) into Eq. (1) and using Eq. (2) yields τ:

$$\tau = \widehat{Q}^k[\psi_k + 2z\xi + 3z^2\eta + \overline{\Psi}_\theta^l(z)\theta_d^l], \tag{9}$$

where $\theta_d^l = [\theta_{,x}^l \;\; \theta_{,y}^l]^{\mathrm{T}}$. For the k_0th layer, denote $u_0(x, y) = u_{k_0}(x, y) = u(x, y, 0)$, $\psi_0(x, y) = \psi_{k_0}(x, y)$. The functions u_k, ψ_k, ξ, η are expressed in terms of u_0 and ψ_0 using the $(L-1)$ conditions each for the continuity of τ and u at the layer interfaces and the two shear traction-free conditions $\tau = 0$ at the top and the bottom surfaces at $z = z_0, z_L$. The continuity condition of τ at the interface $z = z_{i-1}$ between the layers i and $i-1$ is expressed in the following recursive form so that the solution of ψ_i, ξ, η is easily tractable:

$$\begin{aligned} &\widehat{Q}^i[\psi_i + 2z_i\xi + 3z_i^2\eta] + \widehat{Q}^i\overline{\Psi}_\theta^l(z_i)\theta_d^l \\ &\quad = \widehat{Q}^{i-1}[\psi_{i-1} + 2z_{i-1}\xi + 3z_{i-1}^2\eta] + \widehat{Q}^{i-1}\overline{\Psi}_\theta^l(z_{i-1})\theta_d^l + 2\widehat{Q}^i(z_i - z_{i-1})\xi \\ &\quad + 3\widehat{Q}^i(z_i^2 - z_{i-1}^2)\eta + \widehat{Q}^i[\overline{\Psi}_\theta^l(z_i) - \overline{\Psi}_\theta^l(z_{i-1})]\theta_d^l. \end{aligned} \tag{10}$$

Using Eq. (9), the shear traction-free condition $\tau(x,y,z_0)=0$, can also be written in the above pattern as

$$\widehat{Q}^1[\psi_1+2z_1\xi+3z_1^2\eta]+\widehat{Q}^1\overline{\Psi}^l_\theta(z_1)\theta^l_d=2\widehat{Q}^1(z_1-z_0)\xi+3\widehat{Q}^1(z_1^2-z_0^2)\eta+\widehat{Q}^1[\overline{\Psi}^l_\theta(z_1)-\overline{\Psi}^l_\theta(z_0)]\theta^l_d. \quad (11)$$

Adding Eqs. (11) and (10) for $i=2,3,\ldots,k$ yields

$$\widehat{Q}^k(\psi_k+2z_k\xi+3z_k^2\eta)+\widehat{Q}^k\overline{\Psi}^l_\theta(z_k)\theta^l_d=2C^k_1\xi+6C^k_2\eta+C^k_{3l}\theta^l_d,\quad k=2,\ldots,L, \quad (12)$$

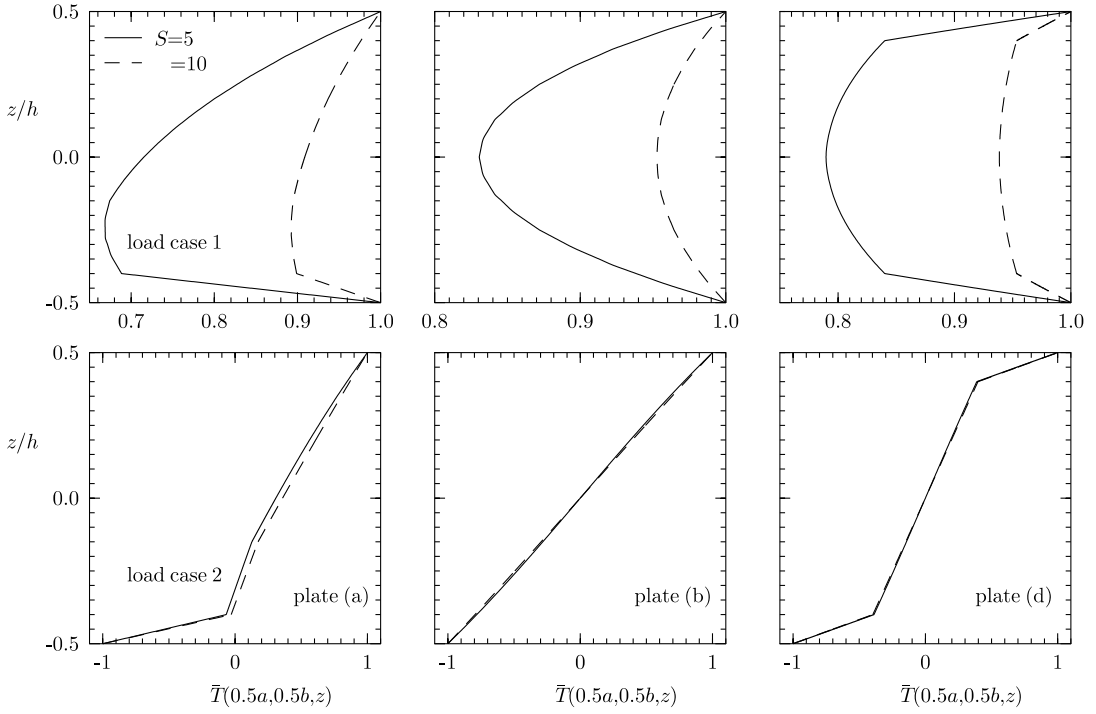

Fig. 2. Temperature distribution for square plates (a), (b) and (d) under load cases 1 and 2.

Table 1
Effect of SCFs on % error of FSDT for plates with $S=10, b/a=1$

Plate	Load	Entity	SCFs		Entity	SCFs		Entity	SCFs	
			5/6	Whitney		5/6	Whitney		5/6	Whitney
(a)	1	$\bar{w}(0.5)$	−72.26	−75.42	$\overline{\sigma}_x(0.5)$	−58.30	−56.53	$\overline{\sigma}_y(0^+)$	7.89	7.96
	2	$\bar{w}(0)$	−15.85	−1.08	$\overline{\sigma}_x(0.5)$	−13.07	−17.88	$\overline{\sigma}_y(0.2^-)$	−1.19	−4.45
(b)	1	$\bar{w}(0.5)$	−100.0	−100.0	$\sigma_x(0.5)$	−10.55	−10.55	$\overline{\sigma}_y(-0.25^+)$	−7.63	−7.63
	2	$\bar{w}(0)$	−0.14	4.67	$\overline{\sigma}_x(0.5)$	−10.38	−12.78	$\overline{\sigma}_y(-0.25^+)$	4.57	11.35
(c)	1	$\bar{w}(0.5)$	−100.0	−100.0	$\overline{\sigma}_x(0.5)$	−25.54	−34.07	$\overline{\sigma}_y(-0.5)$	−25.54	−34.07
	2	$\bar{w}(0)$	−1.89	−1.89	$\overline{\sigma}_x(0.5)$	−4.61	−4.61	$\overline{\sigma}_y(0.5)$	1.54	1.54
(d)	1	$\bar{w}(0.5)$	−100.0	−100.0	$\overline{\sigma}_x(-0.5)$	3.92	3.92	$\overline{\sigma}_y(-0.45^+)$	3.19	3.19
	2	$\bar{w}(0)$	4.72	3.55	$\overline{\sigma}_x(0.45^-)$	−0.02	0.08	$\overline{\sigma}_y(0.5)$	0.09	−0.02

$$C_1^k = \sum_{i=1}^{k} \widehat{Q}^i (z_i - z_{i-1}), \quad C_2^k = \sum_{i=1}^{k} \widehat{Q}^i (z_i^2 - z_{i-1}^2)/2, \quad C_{3l}^k = \sum_{i=1}^{k} \widehat{Q}^i [\overline{\Psi}_\theta^l(z_i) - \overline{\Psi}_\theta^l(z_{i-1})]. \tag{13}$$

Using Eq. (9), the condition $\tau_{zx}(x, y, z_L) = 0$, can be written as

$$\widehat{Q}^L [\psi_L + 2z_L \xi + 3z_L^2 \eta] + \widehat{Q}^L \overline{\Psi}_\theta^l(z_L) \theta_d^l = 0. \tag{14}$$

Eliminating ψ_L from Eqs. (14) and (12) for $k = L$, and rewriting Eq. (11) yields

$$2C_1^L \xi + 6C_2^L \eta = -C_{3l}^L \theta_d^l, \quad 2z_0 \xi + 3z_0^2 \eta = C_5^l \theta_d^l - \psi_1, \tag{15}$$

where $C_5^l = -\overline{\Psi}_\theta^l(z_0)$ and I_2 is a 2×2 identity matrix. The solution of Eq. (15) for ξ, η is

$$\xi = R_3 \psi_1 + R_5^l \theta_d^l, \quad \eta = R_4 \psi_1 + R_6^l \theta_d^l, \tag{16}$$

where

$$\begin{aligned} &\Delta = 4z_0^2 C_1^L - 8z_0 C_2^L, \quad R_3 = 4\Delta^{-1} C_2^L, \quad R_4 = -4\Delta^{-1} C_1^L/3, \\ &R_5^l = -\Delta^{-1}(2z_0^2 C_{3l}^L + 4C_2^L C_5^l), \quad R_6^l = \Delta^{-1}(4z_0 C_{3l}^L + 4C_1^L C_5^l)/3. \end{aligned} \tag{17}$$

Substituting ξ, η from Eq. (16) into Eq. (12) yields

$$\psi_k = R_2^k \psi_1 + R_{l1}^k \theta_d^l, \tag{18}$$

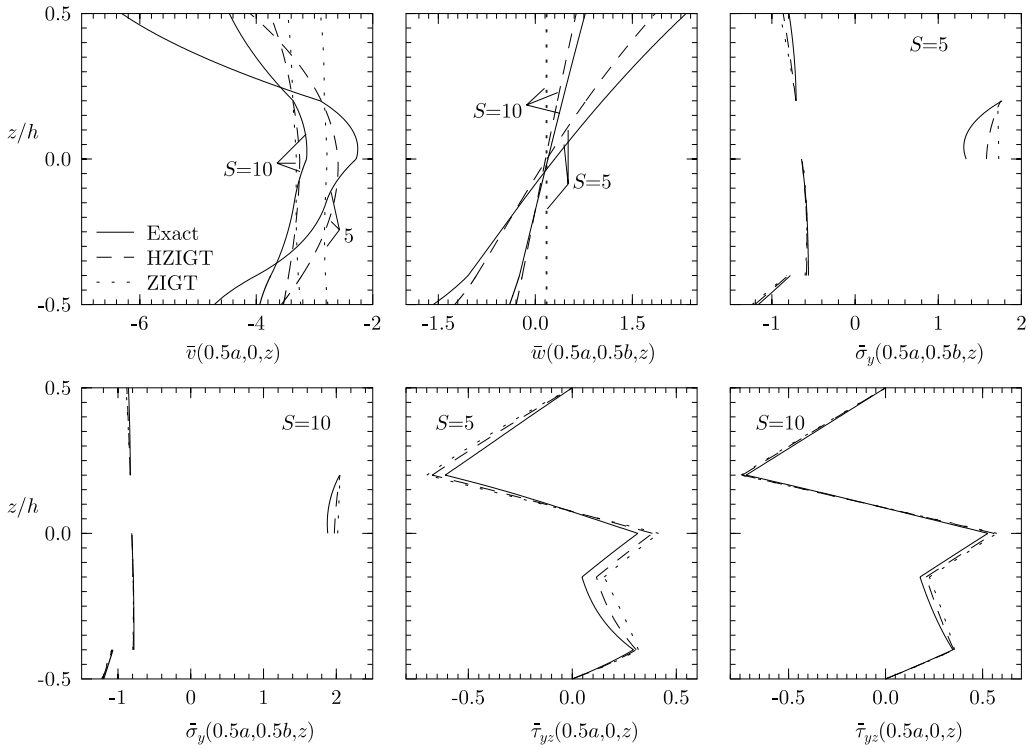

Fig. 3. Distributions of $\bar{v}$, $\bar{w}$, $\overline{\sigma}_y$, $\overline{\tau}_{yz}$ for square test plate (a) under load case 1.

where

$$R_2^k = a_1^k R_3 + a_2^k R_4, \quad R_{l1}^k = a_1^k R_5^l + a_2^k R_6^l + (\widehat{Q}^k)^{-1} C_{3l}^k - \overline{\Psi}_\theta^l(z_k) I_2,$$
$$a_1^k = 2[(\widehat{Q}^k)^{-1} C_1^k - z_k I_2], \quad a_2^k = 3[2(\widehat{Q}^k)^{-1} C_2^k - z_k^2 I_2]. \tag{19}$$

Using Eq. (7), continuity of u between the layers i and $i-1 \Rightarrow u_i + z_{i-1}\psi_i = u_{i-1} + z_{i-1}\psi_{i-1}$ and using Eq. (18):

$$u_i = u_{i-1} + z_{i-1}[(R_2^{i-1} - R_2^i)\psi_1 + (R_{l1}^{i-1} - R_{l1}^i)\theta_d^l], \quad i = 2, \ldots, L. \tag{20}$$

Adding Eq. (20) for $i = 2$ to k yields u_k in terms of u_1:

$$u_k = u_1 + \overline{R}_2^k \psi_1 + \overline{R}_{l1}^k \theta_d^l, \tag{21}$$

$$\overline{R}_2^k = \sum_{i=2}^{k} z_{i-1}(R_2^{i-1} - R_2^i), \quad \overline{R}_{l1}^k = \sum_{i=2}^{k} z_{i-1}(R_{l1}^{i-1} - R_{l1}^i). \tag{22}$$

Eqs. (21) and (18) yield for the k_0th layer:

$$u_0(x,y) = u_{k_0}(x,y) = u_1 + \overline{R}_2^{k_0}\psi_1 + \overline{R}_{l1}^{k_0}\theta_d^l, \quad \psi_0(x,y) = \psi_{k_0}(x,y) = R_2^{k_0}\psi_1 + R_{l1}^{k_0}\theta_d^l. \tag{23}$$

Substituting ξ, η from Eq. (16), u_k from Eq. (21) with u_1 from Eq. $(23)_1$ and ψ_k from Eq. (18) in Eq. (7) yields

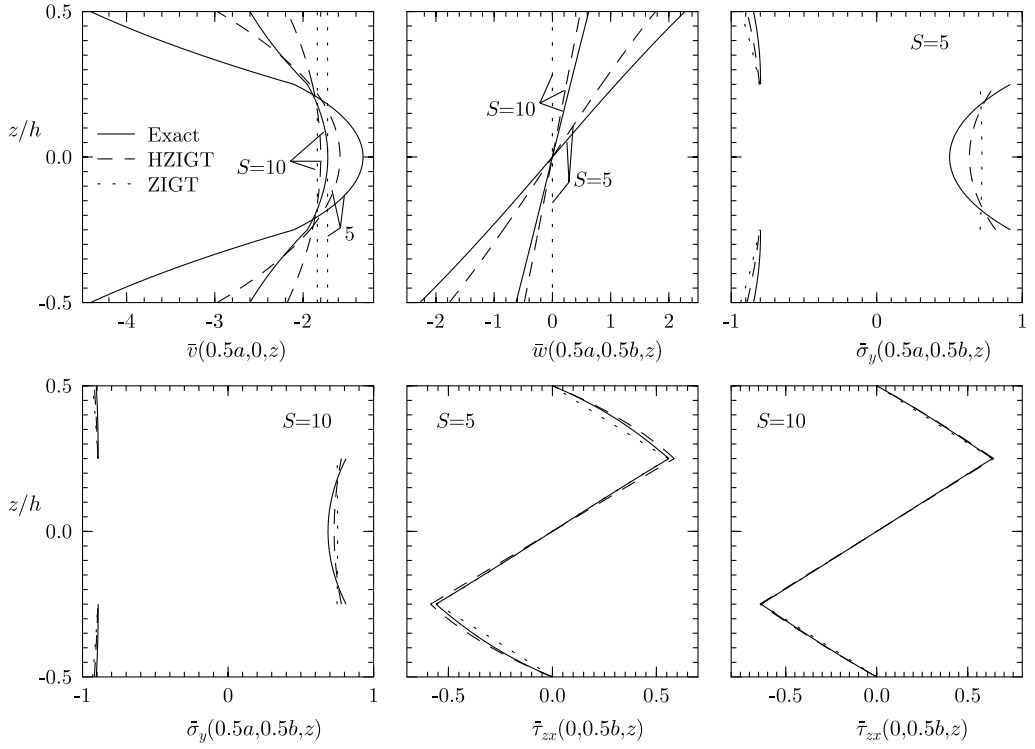

Fig. 4. Distributions of $\bar{v}$, $\bar{w}$, $\overline{\sigma}_y$, $\overline{\tau}_{zx}$ for square composite plate (b) under load case 1.

$$u(x,y,z) = u_0(x,y) - zw_{0_d}(x,y) + R_k(z)\psi_1(x,y) + R^l_{k\theta}(z)\theta^l_d(x,y), \tag{24}$$

where

$$\begin{aligned} &R_k(z) = R^k_1 + zR^k_2 + z^2R_3 + z^3R_4, \quad R^l_{k\theta}(z) = R^{kl}_1 + zR^k_{l1} + z^2R^l_5 + z^3R^l_6, \\ &R^k_1 = \overline{R}^k_2 - \overline{R}^{k_0}_2, \quad R^{kl}_1 = \overline{R}^k_{l1} - \overline{R}^{k_0}_{l1}. \end{aligned} \tag{25}$$

Substituting ψ_1 in terms of ψ_0 from Eq. $(23)_2$ into Eq. (24) yields the expression of u as

$$u(x,y,z) = u_0(x,y) - zw_{0_d}(x,y) + R^k(z)\psi_0(x,y) + \overline{R}^{kl}(z)\theta^l_d(x,y), \tag{26}$$

where

$$\begin{aligned} &R^k(z) = R_k(z)(R^{k_0}_2)^{-1} = \hat{R}^k_1 + z\hat{R}^k_2 + z^2\hat{R}_3 + z^3\hat{R}_4, \\ &\overline{R}^{kl}(z) = R^l_{k\theta}(z) - R^k(z)R^{k_0}_{l1} = \widehat{R}^{kl}_1 + z\widehat{R}^k_{l1} + z^2\widehat{R}^l_5 + z^3\widehat{R}^l_6, \\ &(\widehat{R}^k_1, \widehat{R}^k_2, \widehat{R}_3, \widehat{R}_4) = (R^k_1, R^k_2, R_3, R_4)(R^{k_0}_2)^{-1}, \\ &\widehat{R}^{kl}_1 = R^{kl}_1 - \widehat{R}^k_1R^{k_0}_{l1}, \quad \widehat{R}^k_{l1} = R^k_{l1} - \widehat{R}^k_2R^{k_0}_{l1}, \quad \widehat{R}^l_5 = R^l_5 - \widehat{R}_3R^{k_0}_{l1}, \quad \widehat{R}^l_6 = R^l_6 - \widehat{R}_4R^{k_0}_{l1}. \end{aligned} \tag{27}$$

R^k, R^{kl} are diagonal matrices. Thus w, u are related to the the primary variables u_0, w_0, ψ_0 and θ^l by Eqs. (6) and (26). The number of the mechanical primary variables is five which is the same as in the FSDT and the TOT. Since σ_z has been neglected in the present formulation, like most other 2D theories including FSDT and TOT, the condition of continuity of σ_z at the layer interfaces is not satisfied.

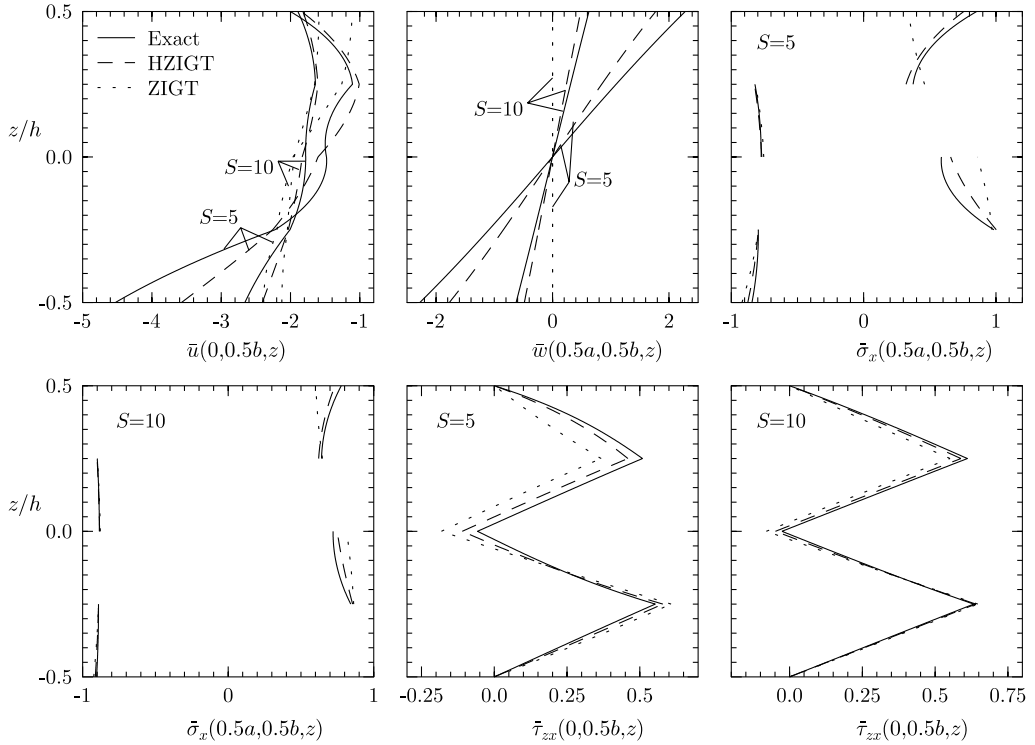

Fig. 5. Distributions of $\bar{u}$, $\bar{w}$, $\bar{\sigma}_x$, $\bar{\tau}_{zx}$ for square composite plate (c) under load case 1.

3. Governing equations of HZIGT

Let A be the surface area of the plate. Denoting $\langle\cdots\rangle = \sum_{k=1}^{L}\int_{z_{k-1}^{+}}^{z_k^{-}}(\ldots)\,\mathrm{d}z$, the principle of virtual work can be expressed as

$$\int_A [\langle \sigma_x\,\delta\varepsilon_x + \sigma_y\,\delta\varepsilon_y + \tau_{xy}\,\delta\gamma_{xy} + \tau_{yz}\,\delta\gamma_{yz} + \tau_{zx}\,\delta\gamma_{zx}\rangle]\,\mathrm{d}A - \int_{\Gamma_L}\langle \sigma_n\,\delta u_n + \tau_{ns}\,\delta u_s + \tau_{nz}\,\delta w\rangle\,\mathrm{d}s = 0 \tag{28}$$

$\forall\,\delta u_0, \delta w_0, \delta\psi_0$. Γ_L is the boundary curve of the mid-plane of the plate with normal n, tangent s and enclosed area A. This variational equation is expressed in terms of δu_0, δw_0, $\delta\psi_0$ and the stress resultants to yield equilibrium equations and boundary conditions. The stress resultants N, M, P, Q, V are defined by

$$\begin{aligned} &N = [\,N_x \quad N_y \quad N_{xy}\,]^{\mathrm{T}}, \quad M = [\,M_x \quad M_y \quad M_{xy}\,]^{\mathrm{T}}, \quad P = [\,P_x \quad P_{yx} \quad P_{xy} \quad P_y\,]^{\mathrm{T}},\\ &Q = [\,Q_x \quad Q_y\,]^{\mathrm{T}}, \quad V = [\,V_x \quad V_y\,]^{\mathrm{T}}, \end{aligned} \tag{29}$$

$$F_1 = [\,N^{\mathrm{T}} \quad M^{\mathrm{T}} \quad P^{\mathrm{T}}\,]^{\mathrm{T}} = [\langle f^{\mathrm{T}}\sigma\rangle], \quad [Q, V] = \left\langle \left[R_{,z}^{k\mathrm{T}}(z), I_2\right]\tau \right\rangle, \tag{30}$$

where $f = [I_3 \;\; zI_3 \;\; \Phi^k]$, I_n is a $n \times n$ identity matrix and

$$\Phi^k = \begin{bmatrix} R_{11}^k & 0 & 0 & 0 \\ 0 & 0 & 0 & R_{22}^k \\ 0 & R_{11}^k & R_{22}^k & 0 \end{bmatrix}. \tag{31}$$

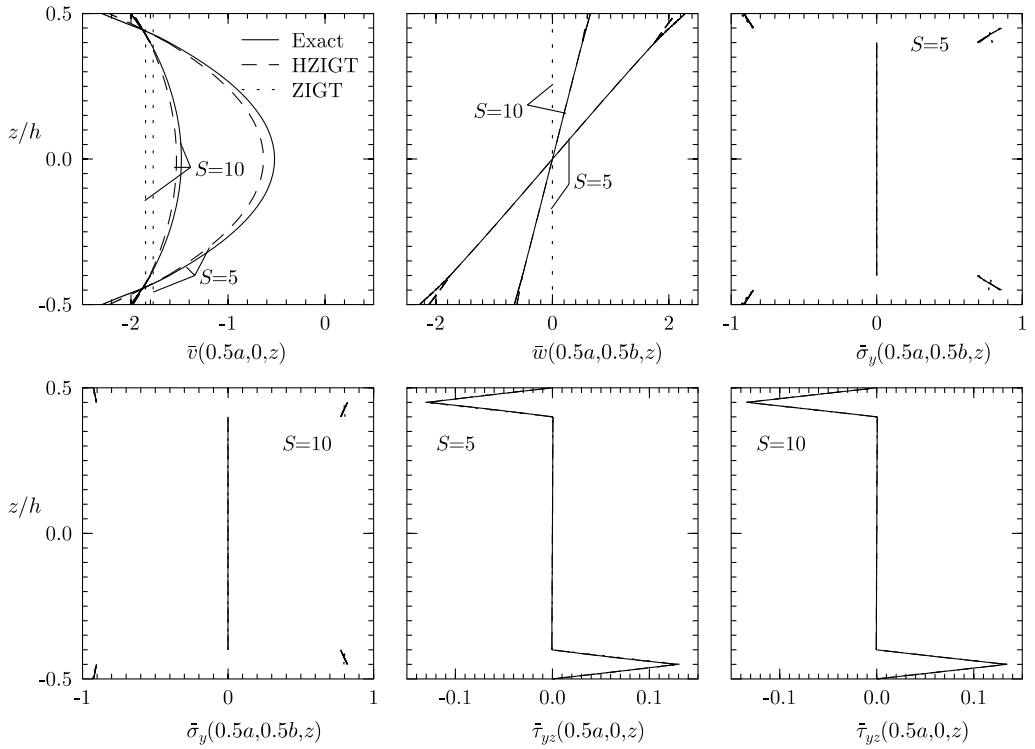

Fig. 6. Distributions of $\bar{v}$, $\bar{w}$, $\bar{\sigma}_y$, $\bar{\tau}_{yz}$ for square sandwich plate (d) under load case 1.

It can be shown that the elements of R^k, N, M, P transform as second order tensors and the elements of V, Q transform as vectors for the coplanar axes x, y and n, s.

Using expressions of w, u from Eqs. (6), (26) and using Eq. (30), the area integral in Eq. (28) becomes

$$\int_A \left[\delta\bar{\varepsilon}_1^{\mathrm{T}} F_1 + \delta\bar{\varepsilon}_2^{\mathrm{T}} Q\right] \mathrm{d}A, \tag{32}$$

where

$$\begin{aligned} \bar{\varepsilon}_1 &= [\, u_{0_x,x} \quad u_{0_y,y} \quad u_{0_x,y} + u_{0_y,x} \quad -w_{0,xx} \quad -w_{0,yy} \quad -2w_{0,xy} \quad \psi_{0_x,x} \quad \psi_{0_x,y} \quad \psi_{0_y,x} \quad \psi_{0_y,y}\,]^{\mathrm{T}}, \\ \bar{\varepsilon}_2 &= [\, \psi_{0_x} \quad \psi_{0_y}\,]^{\mathrm{T}}. \end{aligned} \tag{33}$$

Using Eq. (26), the relation for the components n, s can be expressed as

$$\begin{bmatrix} \delta u_n \\ \delta u_s \end{bmatrix} = \begin{bmatrix} \delta u_{0_n} \\ \delta u_{0_s} \end{bmatrix} - z \begin{bmatrix} \delta w_{0,n} \\ \delta w_{0,s} \end{bmatrix} + \begin{bmatrix} R^k_{nn} & R^k_{ns} \\ R^k_{sn} & R^k_{ss} \end{bmatrix} \begin{bmatrix} \delta\psi_{0_n} \\ \delta\psi_{0_s} \end{bmatrix} + \begin{bmatrix} R^{kl}_{nn} & R^{kl}_{ns} \\ R^{kl}_{sn} & R^{kl}_{ss} \end{bmatrix} \begin{bmatrix} \delta\theta^l_{,n} \\ \delta\theta^l_{,s} \end{bmatrix}. \tag{34}$$

Using the expressions of w, u from Eqs. (6), (26) and the stress resultant components for axes n, s defined analogous to Eq. (30), the line integral in Eq. (28) can be expressed, using Eq. (34), as

$$\int_{\Gamma_L} [N_n\,\delta u_{0_n} + N_{ns}\,\delta u_{0_s} - M_n\,\delta w_{0,n} + (V_n + M_{ns,s})\,\delta w_0 + P_n\,\delta\psi_{0_n} + P_{ns}\,\delta\psi_{0_s}]\,\mathrm{d}s + \sum_i \Delta M_{ns}(s_i)\,\delta w_0(s_i) = 0, \tag{35}$$

where the lateral surface has corners at $s = s_i$.

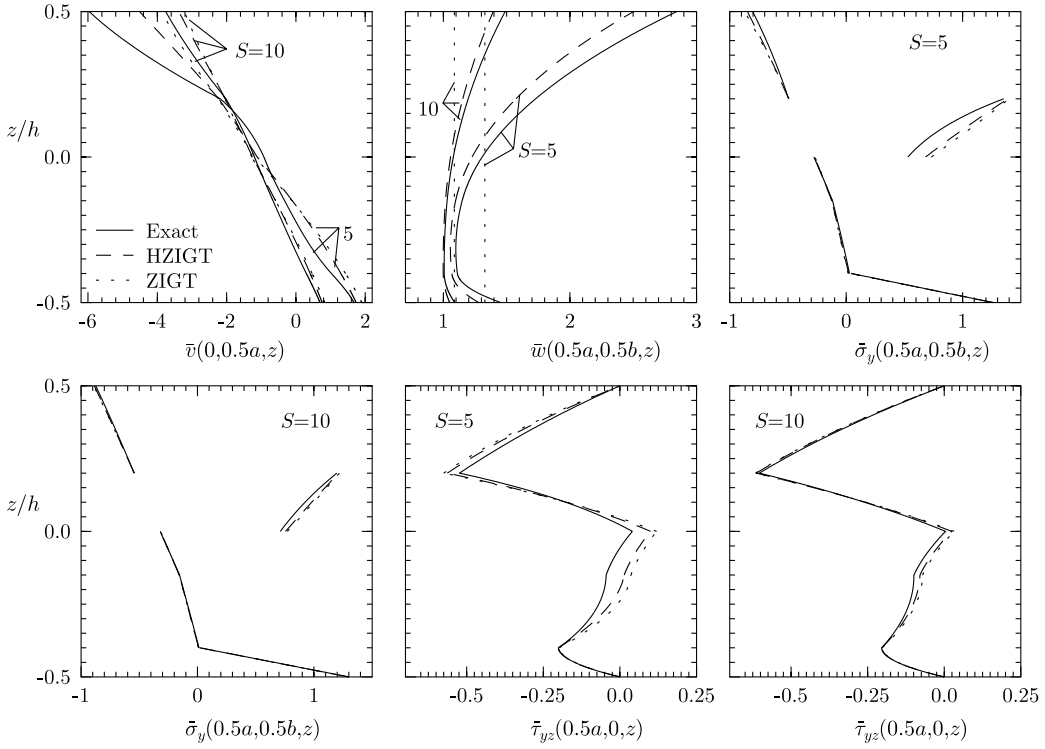

Fig. 7. Distributions of $\bar{v}$, $\bar{w}$, $\bar{\sigma}_y$, $\bar{\tau}_{yz}$ for square test plate (a) under load case 2.

The area integral in Eq. (32) is expressed in terms of δu_{0_x}, δu_{0_y}, δw_0, $\delta\psi_{0_x}$, $\delta\psi_{0_y}$ by using Green's theorem if required, and the terms involving δu_{0_x}, δu_{0_y}, $\delta\psi_{0_x}$, $\delta\psi_{0_y}$, $\delta w_{0,x}$, $\delta w_{0,y}$ in the integrand of Γ_L are expressed in terms of the components n, s. The details are omitted. Thus Eq. (28) yields the following five equations of equilibrium:

$$\begin{aligned} &-N_{x,x}-N_{xy,y}=0, \quad -N_{xy,x}-N_{y,y}=0, \quad -M_{x,xx}-2M_{xy,xy}-M_{y,yy}=0,\\ &-P_{x,x}-P_{yx,y}+Q_x=0, \quad -P_{xy,x}-P_{y,y}+Q_y=0, \end{aligned} \tag{36}$$

The boundary conditions on Γ_L are the prescribed values of one of the factors of each of the following products:

$$u_{0_n}N_n,\ u_{0_s}N_{ns},\ w_0(V_n+M_{ns,s}),\ w_{0,n}M_n,\ \psi_{0_n}P_n,\ \psi_{0_s}P_{ns}, \quad \text{and at } s_i:\ w_0(s_i)\,\Delta M_{ns}(s_i). \tag{37}$$

The relations between the resultants F_1, F_2 with $\bar{\varepsilon}_1, \bar{\varepsilon}_2$ are obtained by substituting the expressions of σ, τ into Eq. (30):

$$F_1 = A\bar{\varepsilon}_1 + A^l\theta^l_{dd} - \gamma^l\theta^l, \quad Q = \overline{A}\bar{\varepsilon}_2 + \overline{A}^l\theta^l_d, \tag{38}$$

where $\theta^l_{dd} = \left[\theta^l_{,xx}\ \ \theta^l_{,xy}\ \ \theta^l_{,yx}\ \ \theta^l_{,yy}\right]^{\mathrm{T}}$ and the plate stiffness $A[10\times10], \overline{A}[2\times2]$; the plate thermo-mechanical coefficients $A^l[10\times4], \overline{A}^l[2\times2], \gamma^l[10\times1]$ are defined in terms of the material constants by

$$[A, A^l] = \langle f^{\mathrm{T}}(z)\overline{Q}[f(z), \overline{\Phi}^{kl}(z)]\rangle, \quad \gamma^l = \langle f^{\mathrm{T}}(z)\bar{\beta}\Psi^l_\theta(z)\rangle, \quad [\overline{A}, \overline{A}^l] = \left\langle R^{k^{\mathrm{T}}}_{,z}(z)\widehat{Q}\left[R^{k^{\mathrm{T}}}_{,z}, \overline{\Gamma}^{kl}(z)\right]\right\rangle, \tag{39}$$

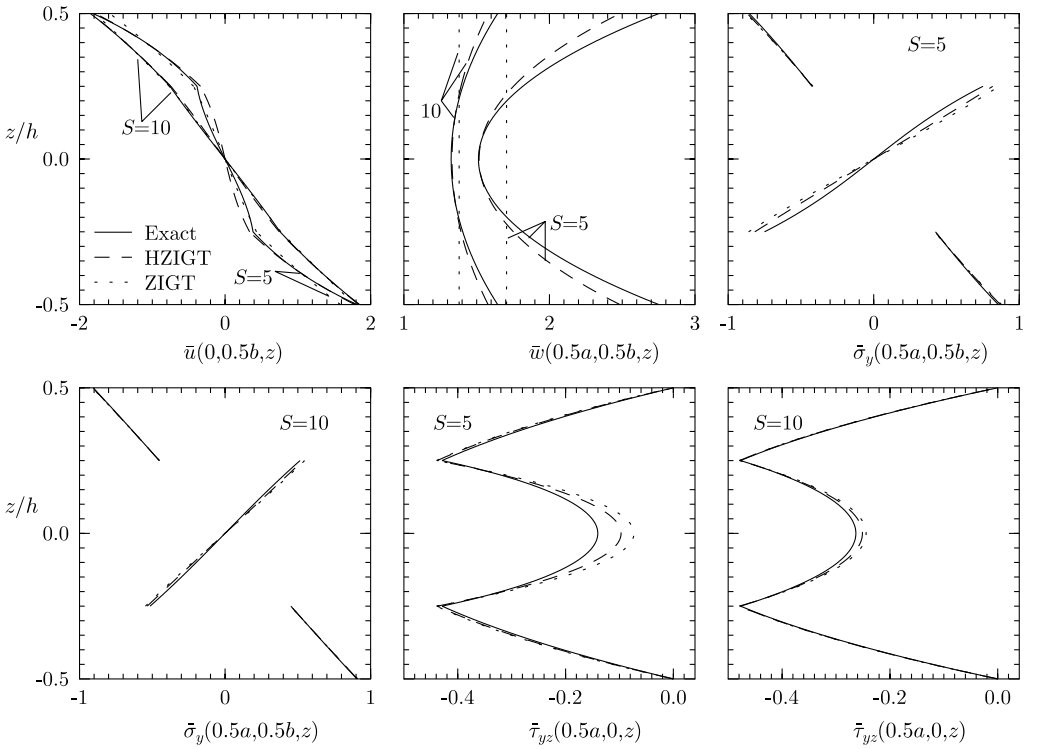

Fig. 8. Distributions of $\bar{u}$, $\bar{w}$, $\bar{\sigma}_y$, $\bar{\tau}_{yz}$ for square composite plate (b) under load case 2.

with

$$\overline{\Phi}^{kl} = \begin{bmatrix} \overline{R}^{kl}_{11} & 0 & 0 & 0 \\ 0 & 0 & 0 & \overline{R}^{kl}_{22} \\ 0 & \overline{R}^{kl}_{11} & \overline{R}^{kl}_{22} & 0 \end{bmatrix}, \quad \Gamma^{kl}(z) = \overline{R}^{kl}_{,z}(z) + \overline{\Psi}^{l}_{\theta}(z) I_2, \tag{40}$$

$$A = \begin{bmatrix} A_{11} & A_{12} & \dots & A_{1,10} \\ A_{21} & A_{22} & \dots & A_{2,10} \\ \vdots & \vdots & \vdots & \vdots \\ A_{10,1} & A_{10,2} & \dots & A_{10,10} \end{bmatrix} = A^{\mathrm{T}}, \quad A^l = \begin{bmatrix} A^l_{11} & A^l_{12} & A^l_{13} & A^l_{14} \\ A^l_{21} & A^l_{22} & A^l_{23} & A^l_{24} \\ \vdots & \vdots & \vdots & \\ A^l_{10,1} & A^l_{10,2} & A^l_{10,3} & A^l_{10,4} \end{bmatrix}, \quad \gamma^l = \begin{bmatrix} \gamma^l_1 \\ \gamma^l_2 \\ \vdots \\ \gamma^l_{10} \end{bmatrix}, \tag{41}$$

$$\overline{A} = \begin{bmatrix} \overline{A}_{11} & \overline{A}_{12} \\ \overline{A}_{21} & \overline{A}_{22} \end{bmatrix} = \overline{A}^{\mathrm{T}}, \quad \overline{A}^l = \begin{bmatrix} \overline{A}^l_{11} & \overline{A}^l_{12} \\ \overline{A}^l_{21} & \overline{A}^l_{22} \end{bmatrix}. \tag{42}$$

Substitution of the expressions of the resultants from Eq. (38) into Eq. (36), yields the following equilibrium equations in terms of $\overline{U} = [u_{0_x}\ u_{0_y}\ w_0\ \psi_{0_x}\ \psi_{0_y}]^{\mathrm{T}}$, taking into account the zero elements of $A, \overline{A}, A^l, \overline{A}^l$:

$$L\overline{U} = \overline{P}, \tag{43}$$

where $\overline{P} = [P_1\ P_2\ P_3\ P_4\ P_5]^{\mathrm{T}}$. L is differential operator matrix with $L_{ip} = L_{pi}$ and

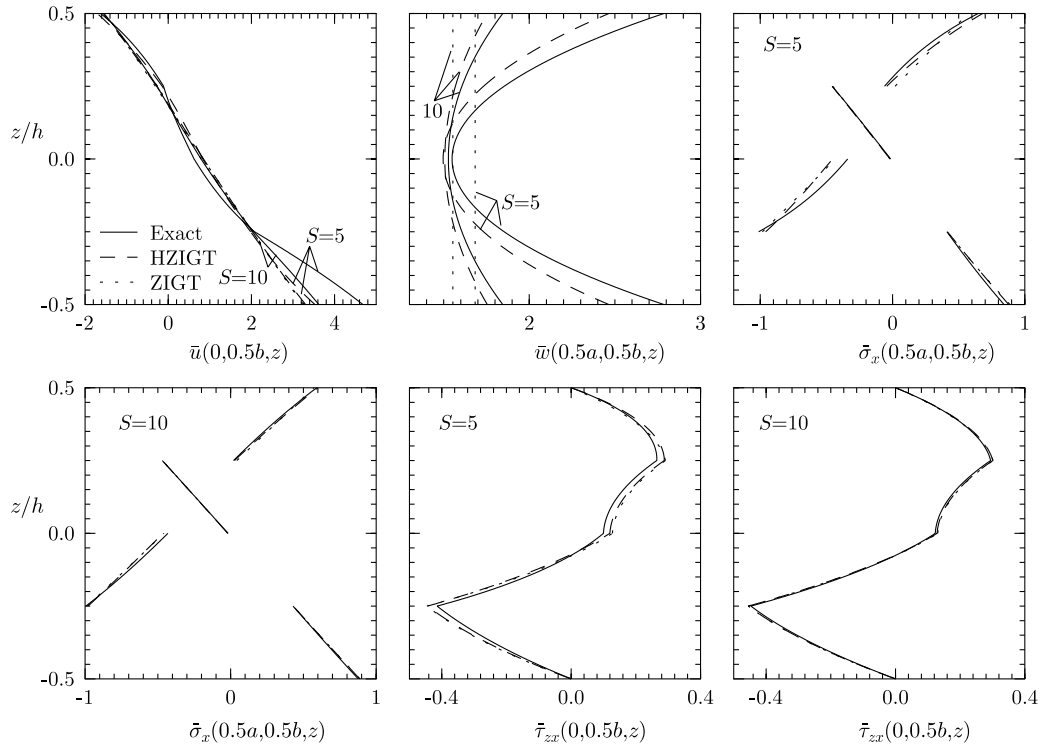

Fig. 9. Distributions of $\bar{u}$, $\bar{w}$, $\overline{\sigma}_x$, $\overline{\tau}_{zx}$ for square composite plate (c) under load case 2.

$$
\begin{aligned}
&L_{11} = -A_{11}()_{,xx} - A_{33}()_{,yy}, \quad L_{12} = -(A_{12} + A_{33})()_{,xy},\\
&L_{13} = A_{14}()_{,xxx} + (A_{15} + 2A_{36})()_{,xyy}, \quad L_{14} = -A_{17}()_{,xx} - A_{38}()_{,yy},\\
&L_{15} = -(A_{1,10} + A_{39})()_{,xy}, \quad L_{22} = -A_{22}()_{,yy} - A_{33}()_{,xx},\\
&L_{23} = (A_{24} + 2A_{36})()_{,xxy} + A_{25}()_{,yyy},\\
&L_{24} = -(A_{27} + A_{38})()_{,xy}, \quad L_{25} = -A_{39}()_{,xx} - A_{2,10}()_{,yy},\\
&L_{33} = -A_{44}()_{,xxxx} - (A_{45} + A_{54} + 4A_{66})()_{,xxyy} - A_{55}()_{,yyyy},\\
&L_{34} = A_{47}()_{,xxx} + (A_{57} + 2A_{68})()_{,xyy}, \quad L_{35} = (A_{4,10} + 2A_{69})()_{,xxy} + A_{5,10}()_{,yyy},\\
&L_{44} = \overline{A}_{11} - A_{77}()_{,xx} - A_{88}()_{,yy}, \quad L_{45} = -(A_{7,10} + A_{89})()_{,xy},\\
&L_{55} = \overline{A}_{22} - A_{10,10}()_{,yy} - A_{99}()_{,xx},
\end{aligned}
\tag{44}
$$

$$
\begin{aligned}
&P_1 = A^l_{11}\theta^l_{,xxx} + (A^l_{14} + A^l_{32} + A^l_{33})\theta^l_{,xyy} - \gamma^l_1\theta^l_{,x},\\
&P_2 = (A^l_{21} + A^l_{32} + A^l_{33})\theta^l_{,xxy} + A^l_{24}\theta^l_{,yyy} - \gamma^l_2\theta^l_{,y},\\
&P_3 = -A^l_{41}\theta^l_{,xxxx} - (A^l_{44} + A^l_{51} + 2A^l_{62} + 2A^l_{63})\theta^l_{,xxyy} - A^l_{54}\theta^l_{,yyyy} + \gamma^l_4\theta^l_{,xx} + \gamma^l_5\theta^l_{,yy},\\
&P_4 = A^l_{71}\theta^l_{,xxx} + (A^l_{74} + A^l_{82} + A^l_{83})\theta^l_{,xyy} - (\gamma^l_7 + \overline{A}^l_{11})\theta^l_{,x},\\
&P_5 = (A^l_{92} + A^l_{93} + A^l_{10,1})\theta^l_{,xxy} + A^l_{10,4}\theta^l_{,yyy} - (\gamma^l_{10} + \overline{A}^l_{22})\theta^l_{,y}.
\end{aligned}
\tag{45}
$$

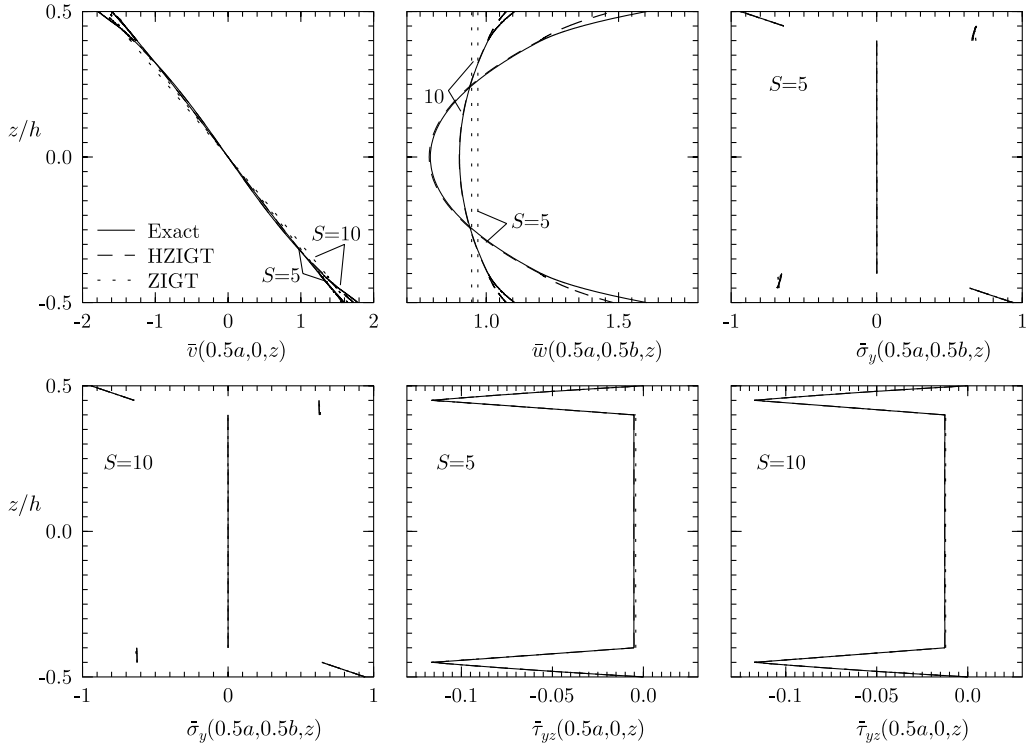

Fig. 10. Distributions of $\bar{v}$, $\bar{w}$, $\bar{\sigma}_y$, $\bar{\tau}_{yz}$ for square sandwich plate (d) under load case 2.

To assess the theory developed herein, by comparison with the 3D exact thermo-elasticity solution, analytical Navier solution is obtained for simply-supported rectangular plates of sides a, b along the axes x, y for the boundary conditions

$$\text{at } x = 0, a : N_x, u_{0_y}, w_0, M_x, P_x, \psi_{0_y} = 0; \quad \text{at } y = 0, b : N_y, u_{0_x}, w_0, M_y, P_y, \psi_{0_x} = 0. \tag{46}$$

The solution is expanded as:

$$\begin{bmatrix} w_0 & \theta^l \\ u_{0_x} & \psi_{0_x} \\ u_{0_y} & \psi_{0_y} \end{bmatrix} = \sum_{n=1}^{\infty}\sum_{m=1}^{\infty} \begin{bmatrix} [w_0 & \theta^l]_{nm} \sin(n\pi x/a)\sin(m\pi y/b) \\ [u_{0_x} & \psi_{0_x}]_{nm} \cos(n\pi x/a)\sin(m\pi y/b) \\ [u_{0_y} & \psi_{0_y}]_{nm} \sin(n\pi x/a)\cos(m\pi y/b) \end{bmatrix}.$$

Eq. (43) yield algebraic equations for n, mth Fourier component. These are not listed for brevity. τ can be obtained using Eq. $(2)_2$ or more accurately by integrating the 3D equations of equilibrium. All transverse stresses in the present study have been computed using the 3D equilibrium equations.

4. Numerical results and assessment

The accuracy of the present theory is assessed by comparison with the exact 3D thermo-elasticity solution (Tungikar and Rao, 1994). The results are also compared with the existing zigzag theory and FSDT in order to assess its improvement over these theories. The shear correction factor for the FSDT solution is taken as 5/6. Four highly inhomogeneous simply-supported plates (a), (b), (c) and (d) are

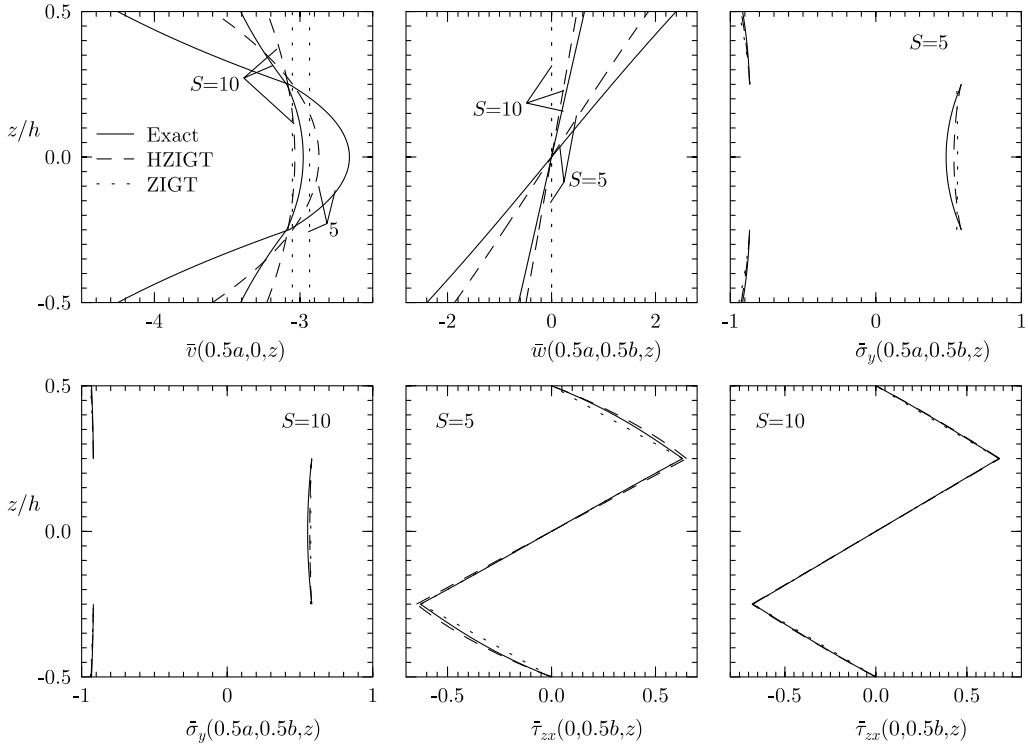

Fig. 11. Distributions of $\bar{v}$, $\bar{w}$, $\bar{\sigma}_y$, $\bar{\tau}_{zx}$ for rectangular ($b/a = 2$) composite plate (b) under load case 1.

selected for the numerical study. The stacking order is mentioned from the bottom. The 5-ply plate (a), which has been devised as a benchmark test case, has plies of thickness $0.1h/0.25h/0.15h/0.2h/0.3h$ of materials $1/2/3/3/3$ with orientations θ_k as [0°/0°/0°/90°/0°], which have highly inhomogeneous properties for stiffness in tension and shear as in Averill and Yip (1996) and highly inhomogeneous coefficients of thermal expansion and thermal conductivities. Plates (b) and (c) are graphite-epoxy cross-ply composite plates of material 4 (Xu et al., 1995), consisting of four plies of equal thickness $0.25h$ with symmetric [0°/90°/90°/0°] and anti-symmetric [90°/0°/90°/0°] lay-ups, respectively. The 5-layer sandwich plate (d) has graphite-epoxy faces [0°/90°] and a soft core (Noor and Burton, 1994) with thickness $0.05h/0.05h/0.8h/0.05h/0.05h$. The material properties of materials 1–4 and of the face and the core of the sandwich plate are:

$[(Y_L, Y_T, G_{LT}, G_{TT}), \nu_{LT}, \nu_{TT}, (\alpha_L, \alpha_T), (k_L, k_T)] =$
Material 1: $[(6.9, 6.9, 1.38, 1.38)\ \text{GPa}, 0.25, 0.25, (35.6, 35.6) \times 10^{-6}\ \text{K}^{-1}, (0.12, 0.12)\ \text{W m}^{-1}\,\text{K}^{-1}]$.
Material 2: $[(224.25, 6.9, 56.58, 1.38)\ \text{GPa}, 0.25, 0.25, (0.25, 35.6) \times 10^{-6}\ \text{K}^{-1}, (7.2, 1.44)\ \text{W m}^{-1}\,\text{K}^{-1}]$.
Material 3: $[(172.5, 6.9, 3.45, 1.38)\ \text{GPa}, 0.25, 0.25, (0.57, 35.6) \times 10^{-6}\ \text{K}^{-1}, (1.92, 0.96)\ \text{W m}^{-1}\,\text{K}^{-1}]$.
Material 4: $[(181, 10.3, 7.17, 2.87)\ \text{GPa}, 0.28, 0.33, (0.02, 22.5) \times 10^{-6}\ \text{K}^{-1}, (1.5, 0.5)\ \text{W m}^{-1}\,\text{K}^{-1}]$.
Face: $[(131.1, 6.9, 3.588, 2.3322)\ \text{GPa}, 0.32, 0.49, (0.0225, 22.5) \times 10^{-6}\ \text{K}^{-1}, (1.5, 0.5)\ \text{W m}^{-1}\,\text{K}^{-1}]$.
For the core: $[(Y_1, Y_2, Y_3, G_{12}, G_{23}, G_{31}), \nu_{12}, \nu_{13}, \nu_{23}] = [(0.2208, 0.2001, 2760, 16.56, 455.4, 545.1)\ \text{MPa}, 0.99, 3 \times 10^{-5}, 3 \times 10^{-5}]$, $\alpha_i = 30.6 \times 10^{-6}\ \text{K}^{-1}$, $k_i = 3.0\ \text{W m}^{-1}\,\text{K}^{-1}$,

where L and T denote directions parallel and transverse to the fibres, ν_{LT} is Poisson's ratio for strain in the T direction under uniaxial normal stress in the L direction, and k_L, k_T, k_i are the thermal conductivity coefficients.

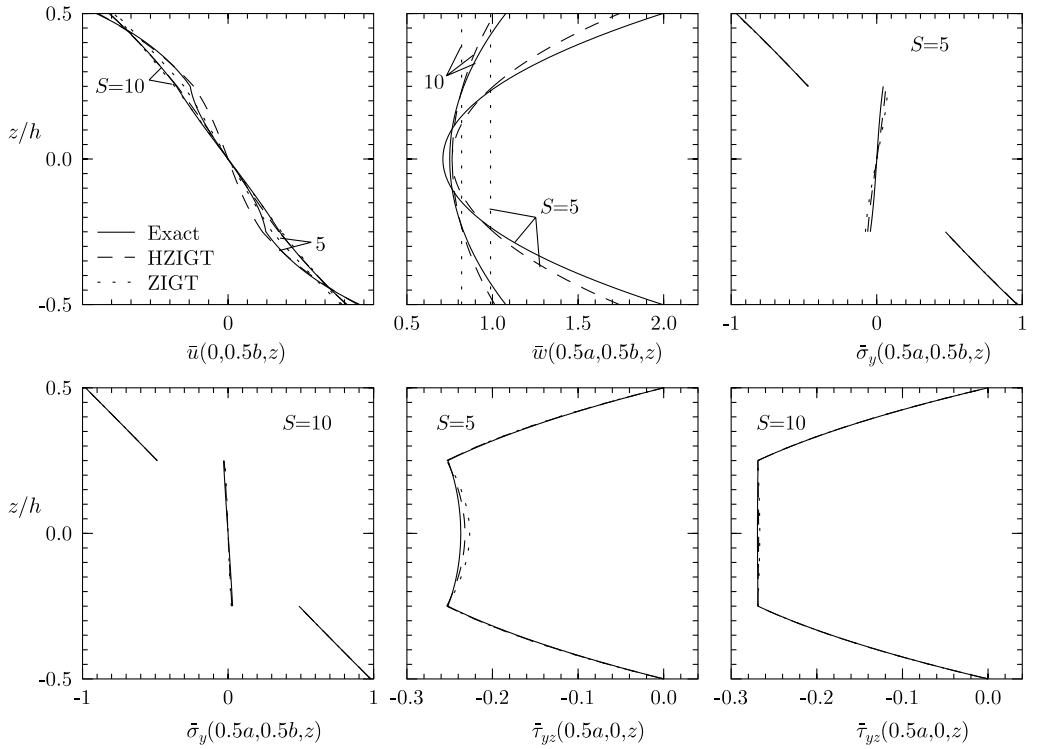

Fig. 12. Distributions of $\bar{u}$, $\bar{w}$, $\bar{\sigma}_y$, $\bar{\tau}_{yz}$ for rectangular ($b/a = 2$) composite plate (b) under load case 2.

Two thermal load cases are considered.

1. Equal temperature rise of the bottom and the top surfaces of the plate with sinusoidal variation: $\theta(x, \pm h/2) = T_0 \sin(\pi x/a) \sin(\pi y/b)$.
2. Equal rise and fall of temperature of the top and bottom surfaces of the plate with sinusoidal variation: $\theta(x, h/2) = -\theta(x, -h/2) = T_0 \sin(\pi x/a) \sin(\pi y/b)$.

For the symmetric laminate, case 1 corresponds to thermal stretching problem with no deflection of the mid-plane and case 2 corresponds to thermal bending problem. The results are non-dimensionalised as follows with $S = a/h$ and with the respective values of Y_T and α_T for plates (a), (b), (c) and those of the face material for plate (d):

$$(\bar{u}, \bar{v}, \bar{w}) = 100(u_x, u_y, w/S)/\alpha_T S h T_0, \quad (\overline{\sigma}_x, \overline{\sigma}_y) = (\sigma_x, \sigma_y)/\alpha_T Y_T T_0,$$
$$(\overline{\tau}_{yz}, \overline{\tau}_{zx}, \overline{\sigma}_z) = (\tau_{yz}, \tau_{zx}, S\sigma_z) S/\alpha_T Y_T T_0, \quad \overline{T} = T/T_0.$$

The 3D thermal problem is solved exactly by exact analytical solution of the heat conduction equation for all the layers and exact satisfaction of the thermal boundary conditions at the top, bottom and four sides, and the continuity conditions at the layer interfaces for temperature and heat flow. The distributions of temperature across the thickness, for the two thermal load cases are given in Fig. 2. These cover a wide range of temperature profiles with large discontinuities in its slope at the layer interfaces in some cases and constitute ideal lay-ups and thermal load cases for assessment of 2D theories. The benchmark test plate (a),

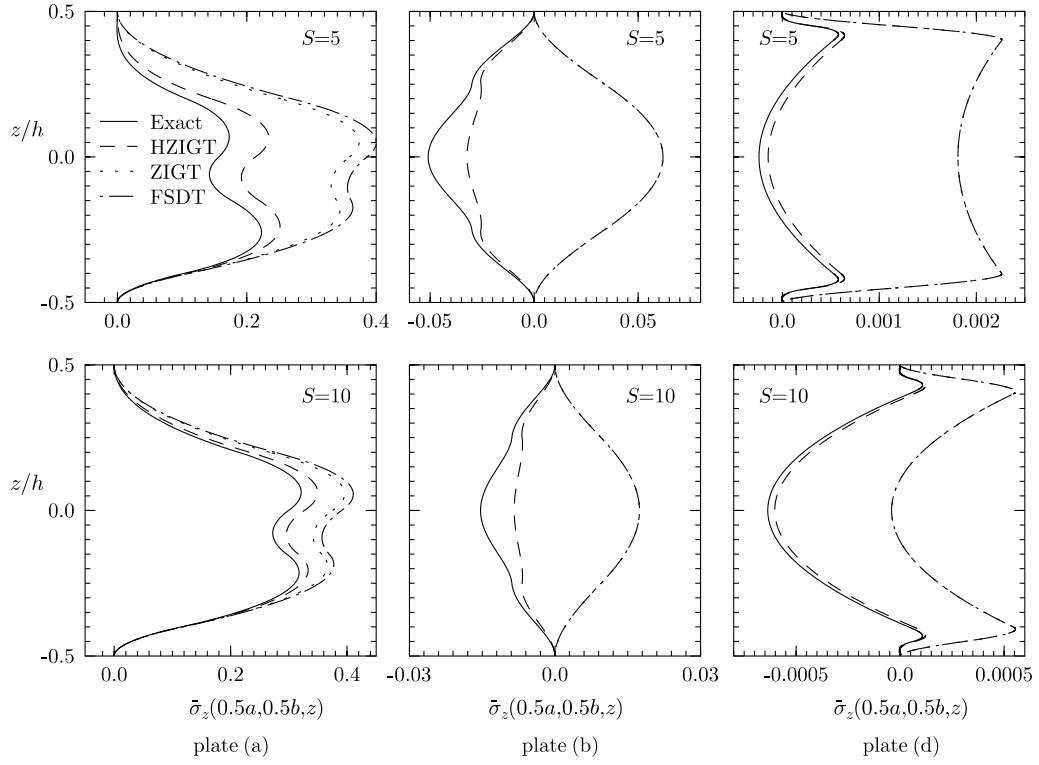

Fig. 13. Distributions of $\overline{\sigma}_z$ for square plates (a), (b) and (d) under load case 1.

devised for this study, does indeed simulate the case of highly non-linear temperature distribution with large discontinuities in its slope. For the present zigzag theory (HZIGT), each layer is divided into r sub-layers for the discretisation of the temperature field across the thickness. Hence, for a plate of L plies, the number n_θ of interpolation points in Eq. (5) equals $rL+1$. The values of $\theta_l(x,y)$ used in Eq. (5) for piecewise linear discretisation of θ are obtained from the values θ^l of the 3D analytical thermal solution at these n_θ interpolation points, i.e., $\theta^l(x,y) = \theta^l \sin(\pi x/a)\sin(\pi y/b)$. Convergence studies have revealed that accurate results are obtained by approximating the exact temperature distributions across the thickness by sub-layer-wise linear distributions with eight equal sub-layers in the core of sandwich plate and four equal sub-layers in each ply for all other layers. As mentioned in the introduction, the ZIGT results are obtained from the formulation of HZIGT by setting $\alpha_3 = 0$ for all the layers.

The accuracy of FSDT depends on shear correction factors (SCFs). The deflection and the inplane stresses in the middle cross-section, at locations across the thickness where these are large, are computed with a constant SCF of 5/6 and with lay-up dependent values according to the method suggested by Whitney (1973). The % errors with respect to the exact 3D solution are compared in Table 1 for square plates (a), (b), (c), (d) with $S = 10$. Non-dimensional coordinate z/h are used for tabulating the results. It is observed that except for a very few cases, the FSDT results with the constant SCF of 5/6 are either identical to or better than the results with the lay-up dependent SCFs. Hence all subsequent results for FSDT have been reported with the constant SCF of 5/6.

The thickness distributions of $\bar{v}$, $\overline{\tau}_{yz}$ at the end and of $\bar{w}$, $\overline{\sigma}_y$ at the centre, obtained by the present zigzag theory (HZIGT), are compared with the exact 2D thermo-elasticity solution and the existing zigzag theory (ZIGT) in Fig. 3 for thermal load case 1 for thick ($S = 5$) and moderately thick ($S = 10$) square test plate

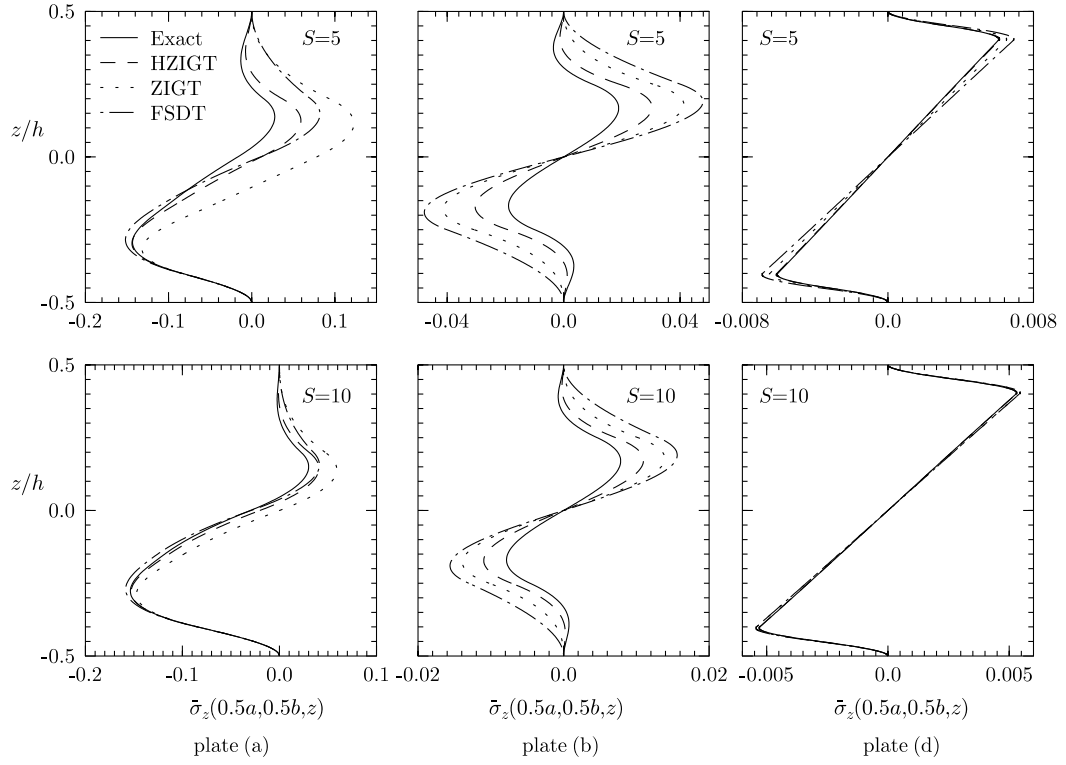

Fig. 14. Distributions of $\overline{\sigma}_z$ for square plates (a), (b) and (d) under load case 2.

(a). Similar results for stresses and displacements for square plates (b), (c), (d) for load case 1 are presented in Figs. 4–6, respectively. The results for the four square plates for load case 2 are compared in Figs. 7–10. The results for the rectangular plate (b) with $b/a = 2$ are compared in Figs. 11 and 12 for the two load cases. The distributions of inplane displacements $\bar{u}$, $\bar{v}$ for the present HZIGT and ZIGT for plates (a), (b), (c) under thermal load 1, have large errors in some layers for $S = 5, 10$, with the errors decreasing with the increase in S but the HZIGT distributions are superior to the ZIGT distributions. The HZIGT distributions of $\bar{v}$ in Fig. 6 for the sandwich plates (d) under thermal load 1 are very accurate, whereas the ZIGT distributions have large qualitative and quantitative errors. The corresponding errors in the distributions of inplane displacements $\bar{u}, \bar{v}$ for thermal load 2 in Figs. 7–10 and 12, for both HZIGT and ZIGT, are relatively much smaller compared to load case 1.

The distributions of the transverse displacement $\bar{w}$ across the thickness for the present HZIGT are in excellent qualitative agreement with the exact 3D thermo-elasticity solution for all the plates with $S = 10, 5$ in both load cases, with small quantitative error for the central deflection. The uniform distributions of $\bar{w}$ for the existing ZIGT are highly erroneous for all the cases. The $\bar{w}$ distributions of the present HZIGT in both the load cases have the least error for the sandwich plate (d), while the maximum error in load case 1 is for the symmetric composite plate (b) and in load case 2 it is for the anti-symmetric composite plate (c).

Table 2
Exact results and % error of HZIGT, ZIGT and FSDT for square plate (a)

S		Load case 1					Load case 2			
		Exact	HZIGT	ZIGT	FSDT		Exact	HZIGT	ZIGT	FSDT
5	$\bar{w}(-0.5h)$	−1.58020	−20.96	−111.30	−115.79	$\bar{w}(0)$	1.30610	−6.08	1.65	−36.97
10		−0.39888	−25.70	−142.07	−153.67		1.07840	−2.01	0.75	−15.85
20		0.02587	108.08	595.09	655.29		0.98267	−0.55	0.30	−4.85
40		0.14609	4.91	26.95	29.83		0.95470	−0.14	0.08	−1.29
5	$\bar{w}(0.5h)$	2.33110	−20.51	−92.34	−89.30	$\bar{w}(0.5h)$	2.84540	−12.00	−53.34	−71.07
10		0.77178	−18.16	−78.26	−72.26		1.48500	−6.11	−26.84	−38.89
20		0.33507	−10.77	−46.34	−41.69		1.08720	−2.22	−9.37	−14.00
40		0.22452	−4.04	−17.40	−15.52		0.98096	−0.62	−2.60	−3.93
5	$\bar{\sigma}_x(0.5h)$	0.67988	−0.07	−77.92	−83.70	$\bar{\sigma}_x(0.5h)$	0.89136	1.80	−34.77	−41.80
10		0.34409	−6.54	−53.11	−58.30		0.80366	−0.83	−12.06	−13.07
20		0.19963	−4.12	−25.53	−28.37		0.78489	−0.33	−3.31	−3.40
40		0.15644	−1.44	−8.39	−9.36		0.78101	−0.09	−0.85	−0.86
5	$\bar{\sigma}_y(0^+)$	1.33650	18.20	29.24	30.30	$\bar{\sigma}_y(0.2h^-)$	1.35310	2.52	3.35	1.05
10		1.88250	4.80	7.25	7.89		1.19680	1.22	1.86	−1.19
20		2.08710	1.23	1.83	2.03		1.12410	0.39	0.61	−0.54
40		2.14520	0.31	0.46	0.51		1.10200	0.10	0.16	−0.16
5	$\bar{\tau}_{xy}(-0.4h^+)$	−1.15700	−15.42	−33.21	−39.29	$\bar{\tau}_{xy}(-0.4h^+)$	0.45737	8.68	23.62	−0.87
10		−1.07610	−6.50	−13.40	−16.91		0.29240	6.23	14.52	−4.59
20		−1.00600	−2.05	−4.14	−5.37		0.22365	2.38	5.45	−2.36
40		−0.98124	−0.55	−1.11	−1.45		0.20323	0.68	1.55	−0.72
5	$\bar{\tau}_{zx}(0.2h)$	0.26101	−6.36	−28.61	−46.49	$\bar{\tau}_{zx}(0.2h)$	0.37874	−3.29	−8.99	14.20
10		0.20825	−6.66	−18.88	−31.09		0.50042	−1.14	−2.97	5.30
20		0.15947	−3.12	−7.93	−13.15		0.55012	−0.31	−0.80	1.51
40		0.14218	−0.96	−2.38	−3.96		0.56477	−0.08	−0.21	0.39
5	$\bar{\tau}_{yz}(0)$	0.31549	22.20	31.69	45.21	$\bar{\tau}_{yz}(0.2h)$	−0.52367	7.59	9.80	9.78
10		0.52732	5.97	8.76	13.03		−0.60361	1.71	2.16	2.54
20		0.62920	1.55	2.28	3.45		−0.62907	0.41	0.51	0.65
40		0.66082	0.39	0.58	0.87		−0.63595	0.10	0.12	0.16

The distributions of inplane normal stresses $\overline{\sigma}_x, \overline{\sigma}_y$ for the present HZIGT, in both load cases, closely follow the pattern of the distributions for the exact 3D solutions for all the plates and generally have less error compared to the existing ZIGT, with the least error for the sandwich plate (d). The distributions of the post-processed transverse shear stresses $\overline{\tau}_{zx}, \overline{\tau}_{yz}$, obtained by the HZIGT and the ZIGT are quite good for all the plates, with the largest error being at the layer interfaces near the mid-plane. In general, the errors in the transverse shear stresses for the HZIGT are smaller than the errors for the ZIGT.

The distributions of the transverse normal stress σ_z obtained from HZIGT, ZIGT and FSDT are compared with the 3D solution for square plates (a), (b), (d) in Figs. 13 and 14 for load cases 1 and 2 respectively. It is observed that HZIGT yields consistently superior results compared to FSDT and ZIGT for all the plates in both load cases. The distributions in HZIGT are in good qualitative agreement with the 3D solution in all cases. In contrast, even the nature of σ_z is erroneously predicted by FSDT and ZIGT for plates (b) and (d) under load case 1.

The exact 3D thermo-elastic results for displacements and stresses at typical points across the thickness, where they are large, along with the % errors of the present HZIGT, existing ZIGT, and FSDT, are given in Tables 2–6 for the four plates under two thermal load cases for $S = 5, 10, 20, 40$. The errors in the FSDT for

Table 3
Exact results and % error of HZIGT, ZIGT and FSDT for square plate (b)

S		Load case 1					Load case 2			
		Exact	HZIGT	ZIGT	FSDT		Exact	HZIGT	ZIGT	FSDT
5	$\bar{w}(-0.5h)$	−2.27770	−22.13	−100.00	−100.00	$\bar{w}(-0.5h)$	2.75290	−9.70	−38.03	−43.02
10		−0.62558	−22.59	−100.00	−100.00		1.64490	−4.01	−16.10	−19.56
20		−0.16040	−22.70	−100.00	−100.00		1.31550	−1.24	−5.04	−6.29
40		−0.04036	−22.73	−100.00	−100.00		1.22830	−0.33	−1.34	−1.69
5	$\bar{w}(0.5h)$	2.27770	−22.13	−100.00	−100.00	$\bar{w}(0)$	1.51260	0.29	12.79	3.70
10		0.62558	−22.59	−100.00	−100.00		1.32500	0.45	4.16	−0.14
20		0.16040	−22.70	−100.00	−100.00		1.23490	0.15	1.16	−0.18
40		0.04036	−22.73	−100.00	−100.00		1.20810	0.05	0.31	−0.05
5	$\bar{\sigma}_x(0.5h)$	0.91338	5.36	−32.64	−32.69	$\bar{\sigma}_x(0.5h)$	0.74627	−2.74	−17.66	−34.78
10		0.80752	1.23	−10.53	−10.55		0.75237	−1.02	−4.88	−10.38
20		0.77529	0.30	−2.84	−2.85		0.76033	−0.28	−1.24	−2.71
40		0.76681	0.07	−0.73	−0.73		0.76299	−0.07	−0.31	−0.68
5	$\bar{\sigma}_y(-0.25h^+)$	0.91864	−11.03	−22.67	−22.72	$\bar{\sigma}_y(-0.25h^+)$	−0.75104	8.89	14.52	13.82
10		0.81083	−3.95	−7.61	−7.63		−0.51518	3.76	6.12	4.57
20		0.77627	−1.09	−2.08	−2.08		−0.41917	1.20	1.95	1.29
40		0.76706	−0.28	−0.53	−0.53		−0.39155	0.32	0.53	0.33
5	$\bar{\tau}_{xy}(-0.5h)$	−0.14263	−20.32	−48.79	−48.82	$\bar{\tau}_{xy}(0.5h)$	−0.13164	−7.54	−14.68	−18.14
10		−0.09955	−8.74	−19.87	−19.89		−0.09746	−2.34	−4.71	−6.72
20		−0.08682	−2.63	−5.90	−5.90		−0.08639	−0.63	−1.30	−1.96
40		−0.08349	−0.70	−1.55	−1.55		−0.08339	−0.16	−0.33	−0.51
5	$\bar{\tau}_{zx}(-0.25h)$	−0.56028	4.58	−0.55	−0.60	$\bar{\tau}_{zx}(0)$	0.19328	−5.71	−4.78	5.38
10		−0.63557	1.09	−0.14	−0.16		0.28502	−1.22	−1.20	1.76
20		−0.65719	0.27	−0.04	−0.04		0.31933	−0.29	−0.29	0.48
40		−0.66280	0.07	−0.01	−0.01		0.32901	−0.07	−0.07	0.12
5	$\bar{\tau}_{yz}(-0.25h)$	0.55527	6.78	11.96	11.90	$\bar{\tau}_{yz}(0)$	−0.14025	−30.78	−47.82	−40.45
10		0.63375	1.77	3.01	2.99		−0.26317	−4.60	−7.20	−4.71
20		0.65669	0.45	0.75	0.75		−0.31303	−0.99	−1.56	−0.89
40		0.66267	0.11	0.19	0.19		−0.32737	−0.24	−0.38	−0.20

$\bar{w}$ are large and the existing ZIGT is only a marginal improvement or a marginal deterioration over FSDT. The errors in $\bar{w}$ for these theories, even for thin plates (a), (b), (c), (d) with $S = 20$ are large, which for ZIGT are 46%, 100%, 100%, 100% for load case 1 and 9.4%, 7.8%, 4.7%, 4.2% for load case 2, respectively. The errors are the largest for the test plate (a). The corresponding errors in $\bar{w}$ for the present HZIGT for $S = 20$ are generally less than one fourth of those, being 10.8%, 22.8%, 22.7%, 6.5% and 2.2%, 1.9%, 1.5%, 0.8% for load cases 1 and 2, respectively. For the moderately thick plate with $S = 10$, the maximum error in $\bar{w}$ for the present HZIGT is 22.7% and 6.1% for load cases 1 and 2. The relative error in $\bar{w}$ at bottom layer of plate (a) for $S = 20$ is large because its exact value itself is very small. It may be noted that there is an error of about 23% in $\bar{w}$ for HZIGT for plates (b) and (c) under load case 1, where the deflection is symmetrical about the mid-plane due to the absence of any bending effect. This error, which does not reduce with higher S is due the contribution of the inplane stresses in the transverse strain which has been neglected in the present theory.

A similar comparison of the results for the inplane stresses $\overline{\sigma}_x, \overline{\sigma}_y, \overline{\tau}_{xy}$ reveals that the existing ZIGT results are only marginally better or marginally worse than the FSDT results except for substantial improvement in $\overline{\sigma}_x$ for plate (b) under load case 2. However, the errors in the stresses for the present

Table 4
Exact results and % error of HZIGT, ZIGT and FSDT for rectangular ($b/a = 2$) plate (b)

S		Load case 1					Load case 2			
		Exact	HZIGT	ZIGT	FSDT		Exact	HZIGT	ZIGT	FSDT
5	$\bar{w}(-0.5h)$	−2.39840	−22.21	−100.00	−100.00	$\bar{w}(-0.5h)$	1.99510	−12.67	−50.44	−51.20
10		−0.63542	−22.71	−100.00	−100.00		1.07800	−5.96	−23.94	−24.60
20		−0.16125	−22.83	−100.00	−100.00		0.83326	−1.94	−7.79	−8.04
40		−0.04046	−22.86	−100.00	−100.00		0.77097	−0.52	−2.11	−2.18
5	$\bar{w}(0.5h)$	2.39840	−22.21	−100.00	−100.00	$\bar{w}(0)$	0.71047	7.57	39.16	37.04
10		0.63542	−22.71	−100.00	−100.00		0.75036	1.97	9.28	8.32
20		0.16125	−22.83	−100.00	−100.00		0.75093	0.50	2.32	2.04
40		0.04046	−22.86	−100.00	−100.00		0.75036	0.13	0.58	0.51
5	$\overline{\sigma}_x(-0.5h)$	1.07560	2.84	−30.72	−30.74	$\overline{\sigma}_x(-0.5h)$	−0.46412	−2.53	−23.45	−34.55
10		0.90381	0.48	−10.05	−10.05		−0.38786	−1.04	−7.50	−11.32
20		0.85455	0.10	−2.72	−2.72		−0.36644	−0.30	−2.02	−3.07
40		0.84180	0.02	−0.69	−0.70		−0.36091	−0.08	−0.52	−0.78
5	$\overline{\sigma}_y(0)$	0.48262	11.15	16.35	16.28	$\overline{\sigma}_y(-0.5h)$	0.96525	0.23	0.53	0.36
10		0.55292	2.68	3.88	3.86		0.97960	0.06	0.13	0.09
20		0.57231	0.66	0.96	0.95		0.98363	0.01	0.03	0.02
40		0.57728	0.16	0.24	0.24		0.98467	0.00	0.01	0.01
5	$\overline{\tau}_{xy}(-0.5h)$	−0.11967	−11.32	−29.43	−29.46	$\overline{\tau}_{xy}(-0.5h)$	0.05294	−5.78	−12.91	−8.34
10		−0.09790	−3.91	−9.74	−9.75		0.03323	−2.31	−5.26	−3.33
20		−0.09185	−1.96	−2.65	−2.65		0.02768	−0.69	−1.59	−1.00
40		−0.09030	−0.68	−0.68	−0.68		0.02625	−0.18	−0.42	−0.26
5	$\overline{\tau}_{zx}(-0.25h)$	−0.63003	3.03	−0.19	−0.21	$\overline{\tau}_{zx}(0)$	0.01013	−16.66	51.43	88.39
10		−0.67639	0.73	−0.06	−0.07		0.02589	−1.29	5.67	9.94
20		−0.68881	0.18	−0.02	−0.02		0.03053	−0.25	1.24	2.19
40		−0.69197	0.04	0.00	0.00		0.03175	−0.06	0.30	0.53
5	$\overline{\tau}_{yz}(-0.25h)$	0.26852	3.21	6.53	6.48	$\overline{\tau}_{yz}(0)$	−0.23707	−2.07	−4.37	−5.80
10		0.28998	0.83	1.64	1.63		−0.26932	−0.48	−0.99	−1.32
20		0.29585	0.21	0.41	0.41		−0.27871	−0.12	−0.24	−0.32
40		0.29736	0.05	0.10	0.10		−0.28115	−0.03	−0.06	−0.08

HZIGT are relatively smaller, often less than half of ZIGT and even one order less in some cases. The errors in the post-processed transverse shear stresses $\overline{\tau}_{yz}, \overline{\tau}_{zx}$ in the existing ZIGT are generally of the same order as in FSDT, whereas the error in the present HZIGT is much smaller except for the greater error in $\overline{\tau}_{zx}$ for plate (b) under load case 1.

5. Conclusions

An efficient new zigzag theory (HZIGT) is presented, based on zigzag third order variation of the in-plane displacements and sub-layer-wise quadratic variation of the transverse displacement accounting explicitly for the thermal contribution to the transverse normal strain. The shear traction-free conditions at the top and the bottom of the plate and the shear continuity conditions at the layer interfaces are satisfied exactly to reduce the primary displacement variables to five. The thermal field is approximated to be piecewise linear across the sub-layers. The present zigzag theory HZIGT is assessed by comparison with the exact 3D thermo-elasticity solution of simply-supported plates for sinusoidal temperature distribution with

Table 5
Exact results and % error of HZIGT, ZIGT and FSDT for square plate (c)

S		Load case 1					Load case 2			
		Exact	HZIGT	ZIGT	FSDT		Exact	HZIGT	ZIGT	FSDT
5	$\bar{w}(-0.5h)$	−2.28010	−22.21	−100.00	−100.00	$\bar{w}(-0.5h)$	2.78690	−11.53	−39.57	−47.18
10		−0.62566	−22.60	−100.00	−100.00		1.84550	−4.90	−15.82	−18.79
20		−0.16040	−22.70	−100.00	−100.00		1.59370	−1.47	−4.65	−5.52
40		−0.04036	−22.73	−100.00	−100.00		1.52960	−0.39	−1.22	−1.44
5	$\bar{w}(0.5h)$	2.28010	−22.21	−100.00	−100.00	$\bar{w}(0)$	1.54920	−3.38	8.71	−4.98
10		0.62566	−22.60	−100.00	−100.00		1.52760	−1.35	1.70	−1.89
20		0.16040	−22.70	−100.00	−100.00		1.51360	−0.38	0.40	−0.52
40		0.04036	−22.73	−100.00	−100.00		1.50950	−0.09	0.10	−0.13
5	$\bar{\sigma}_x(0.5h)$	0.85494	−11.42	−60.07	−72.22	$\bar{\sigma}_x(0.5h)$	0.64727	5.21	−11.00	−15.49
10		0.77709	−5.48	−22.38	−25.54		0.59169	1.23	−3.34	−4.61
20		0.76569	−1.64	−6.30	−6.97		0.57588	0.30	−0.88	−1.21
40		0.76425	−0.43	−1.62	−1.78		0.57180	0.08	−0.22	−0.31
5	$\bar{\sigma}_y(-0.5h)$	0.85494	−11.42	−60.07	−72.22	$\bar{\sigma}_y(0.5h)$	−0.84264	4.22	5.38	5.88
10		0.77709	−5.48	−22.38	−25.54		−0.87679	1.13	1.41	1.54
20		0.76569	−1.64	−6.30	−6.97		−0.88632	0.29	0.36	0.39
40		0.76425	−0.43	−1.62	−1.78		−0.88877	0.07	0.09	0.10
5	$\bar{\tau}_{xy}(-0.5h)$	−0.14288	−17.06	−46.41	−43.56	$\bar{\tau}_{xy}(0.5h)$	−0.13797	−16.98	−24.00	−26.69
10		−0.09958	−7.13	−18.40	−17.04		−0.11299	−5.80	−8.01	−8.86
20		−0.08682	−2.11	−5.39	−4.97		−0.10601	−1.59	−2.19	−2.41
40		−0.08349	−0.55	−1.41	−1.30		−0.10422	−0.41	−0.57	−0.62
5	$\bar{\tau}_{zx}(0.25h)$	0.50909	−9.86	−27.92	−28.18	$\bar{\tau}_{zx}(0.25h)$	0.26478	8.79	10.16	11.75
10		0.61103	−3.64	−9.75	−8.19		0.29420	2.25	2.58	2.95
20		0.64961	−1.03	−2.72	−2.10		0.30246	0.57	0.65	0.74
40		0.66079	−0.26	−0.70	−0.53		0.30459	0.14	0.16	0.18
5	$\bar{\tau}_{yz}(-0.25h)$	−0.50909	−9.86	−27.92	−28.18	$\bar{\tau}_{yz}(0.25h)$	−0.41447	7.09	7.63	8.13
10		−0.61103	−3.64	−9.75	−8.19		−0.44710	1.82	1.95	2.06
20		−0.64961	−1.03	−2.72	−2.10		−0.45608	0.46	0.49	0.52
40		−0.66079	−0.26	−0.70	−0.53		−0.45839	0.11	0.12	0.13

Table 6
Exact results and % error of HZIGT, ZIGT and FSDT for square plate (d)

S		Load case 1					Load case 2			
		Exact	HZIGT	ZIGT	FSDT		Exact	HZIGT	ZIGT	FSDT
5	$\bar{w}(-0.5h)$	−2.28600	−7.10	−100.00	−100.00	$\bar{w}(-0.5h)$	1.60700	−7.88	−39.74	−41.56
10		−0.65442	−6.64	−100.00	−100.00		1.10750	−2.89	−14.69	−14.99
20		−0.16992	−6.51	−100.00	−100.00		0.98211	−0.82	−4.16	−4.18
40		−0.04290	−6.49	−100.00	−100.00		0.95099	−0.21	−1.08	−1.08
5	$\bar{w}(0.5h)$	2.28600	−7.10	−100.00	−100.00	$\bar{w}(0)$	0.78872	−0.53	22.77	19.07
10		0.65442	−6.64	−100.00	−100.00		0.89909	−0.13	5.09	4.72
20		0.16992	−6.51	−100.00	−100.00		0.92977	−0.03	1.23	1.21
40		0.04290	−6.49	−100.00	−100.00		0.93789	−0.01	0.31	0.31
5	$\bar{\sigma}_x(-0.5h)$	0.79731	0.00	−13.67	−13.67	$\bar{\sigma}_x(0.45h^-)$	−0.64546	0.04	−0.05	−0.02
10		0.80447	−0.02	−3.92	−3.92		−0.64855	0.01	−0.01	−0.03
20		0.80683	−0.01	−1.02	−1.02		−0.64870	0.00	0.00	−0.02
40		0.80747	0.00	−0.26	−0.26		−0.64862	0.00	0.00	0.00
5	$\bar{\sigma}_y(-0.45h^+)$	0.85798	−1.13	−10.58	−10.58	$\bar{\sigma}_y(0.5h)$	−0.93567	0.19	0.52	0.38
10		0.82197	−0.34	−3.19	−3.19		−0.94107	0.05	0.13	0.09
20		0.81120	−0.09	−0.84	−0.84		−0.94321	0.01	0.03	0.03
40		0.80837	−0.02	−0.21	−0.21		−0.94389	0.00	0.01	0.01
5	$\bar{\tau}_{xy}(-0.5h)$	−0.06793	−1.74	−16.88	−16.88	$\bar{\tau}_{xy}(-0.5h)$	0.05129	−1.81	−5.90	−5.52
10		−0.06332	−0.52	−5.20	−5.20		0.04909	−0.47	−1.56	−1.33
20		−0.06196	−0.14	−1.38	−1.38		0.04849	−0.12	−0.39	−0.32
40		−0.06161	−0.04	−0.35	−0.35		0.04833	−0.03	−0.10	−0.08
5	$\bar{\tau}_{zx}(-0.45h)$	−0.12147	0.12	−1.87	−1.88	$\bar{\tau}_{zx}(-0.45h)$	0.08171	0.15	−1.20	−4.67
10		−0.13215	0.02	−0.51	−0.51		0.08904	0.05	−0.50	−0.59
20		−0.13539	0.00	−0.13	−0.13		0.09382	0.02	−0.15	0.08
40		−0.13624	0.00	−0.03	−0.03		0.09558	0.01	−0.04	0.05
5	$\bar{\tau}_{yz}(-0.45h)$	0.12851	0.29	2.05	2.05	$\bar{\tau}_{yz}(-0.45h)$	−0.11607	0.25	0.59	0.39
10		0.13383	0.07	0.57	0.57		−0.11727	0.06	0.14	0.09
20		0.13544	0.01	0.14	0.14		−0.11771	0.01	0.03	0.03
40		0.13586	0.00	0.04	0.04		−0.11784	0.00	0.01	0.01

equal temperature rise of the top and bottom surfaces of the plate and with equal rise and fall of temperature of these surfaces. The temperature profiles across the thickness are based on the heat conduction equation. A benchmark test plate, symmetric and anti-symmetric composite plates and sandwich plates are analysed to cover a wide range of temperature profiles across the thickness. It is concluded from the comparative study that the existing ZIGT results are only marginally better (in some cases marginally worse) than those of the FSDT for thermal analysis. The errors are particularly large for deflection even for thin plates with $S = 20$. These theories should not be used for moderately thick plates with $S = 10$ and even for some thin plates with $S = 20$ in which the errors are significant. The present HZIGT yields more accurate results for the deflection and the stresses with few exceptions. The present HZIGT may be used for all types of plates and thermal loadings with small error for $S \geqslant 10$. The new theory generally reproduces quite well the thickness distributions of the inplane normal as well as transverse normal and shear stresses and the transverse displacement for moderately thick plates with relatively small error. The new theory developed herein is more accurate and yet as efficient as the existing zigzag theory and the FSDT, since it is formulated in terms of only five primary displacements. Like TOT and many other HOTs, the finite element implementation of the present theory will require $C^{(1)}$-continuity of the shape functions which prevents

simple element formulations. This can, however, be avoided by using the discrete Kirchhoff technique (Cho et al., 2003).

References

Ali, J.S.M., Bhaskar, K., Varadan, T.K., 1999. A new theory for accurate thermal/mechanical flexural analysis of symmetric laminated plates. Compos. Struct. 45, 227–232.

Argyris, J., Tanek, L., 1997. Recent advances in computational thermostructural analysis of composite plates and shells with strong nonlinearities. Appl. Mech. Rev. 50, 285–306.

Averill, R.C., Yip, Y.C., 1996. An efficient thick beam theory and finite element model with zigzag/sub-laminate approximations. Am. Inst. Aeronaut. Astronaut. J. 34, 1626–1632.

Carrera, E., 2000. An assessment of mixed and classical theories for the thermal stress analysis of orthotropic multi-layered plates. J. Thermal Stresses 23, 797–831.

Carrera, E., 2002. Temperature profile influence on layered plates response considering classical and advanced theories. Am. Inst. Aeronaut. Astronaut. J. 40, 1885–1896.

Cho, M., Oh, J., Kim, J.-S., 2003. Dynamic analysis for delaminated composites using DKQ concept based on higher order zigzag theory. Struct. Dyn. Mat. Conf. 4, 2564–2572.

He, J.F., 1995. Thermoelastic analysis of laminated plates including transverse shear deformation effects. Compos. Struct. 30,, 51–59.

Jonnalagadda, K.D., Tauchert, T.R., Blandford, G.E., 1993. Higher order thermoelastic composite plate theories, analytical comparison. J. Thermal Stresses 16, 265–284.

Kant, T., Khare, R.K., 1994. Finite element thermal stress analysis of composite laminates using a higher order theory. J. Thermal Stresses 17, 229–255.

Kapuria, S., Dumir, P.C., Ahmed, A., 2003. An efficient higher order zigzag theory for composite and sandwich beams for thermal load. Int. J. Solids Struct. 40/24, 6613–6631.

Kheider, A.A., Reddy, J.N., 1991. Thermal stresses and deflection of cross-ply laminated plates using refined theories. J. Thermal Stresses 14, 419–438.

Locke, J.E., 1997. Thermomechanical stress analysis of inhomogeneous antisymmetric cross-ply laminates. Comput. Struct. 62,, 25–34.

Murakami, H., 1993. Assessment of plate theories for treating the thermomechanical response of layered composite plates. Compos. Eng. 3, 137–149.

Nemrovskii, Y.V., 1972. On the theory of thermoelastic bending of reinforced shells and plates. Mech. Compos. Mat. 8,, 750–759.

Noor, A.K., Burton, W.S., 1992. Computational models for high temperature multi-layered composite plates and shells. Appl. Mech. Rev. 45, 419–446.

Noor, A.K., Burton, W.S., 1994. Three-dimensional solutions for initially stressed structural sandwiches. J. Eng. Mech. ASCE 120, 284–303.

Noor, A.K., Malik, M., 1999. Accurate determination of transverse normal stresses in sandwich panels subjected to thermomechanical loading. Comput. Meth. Appl. Mech. Eng. 178, 431–443.

Noor, A.K., Malik, M., 2000. An assessment of modelling approaches for thermo-mechanical stress analysis of laminated composite panels. Comput. Mech. 25, 43–58.

Park, J.W., Kim, Y.H., 2002. Re-analysis procedure for laminated plates using FSDT finite element method. Comput. Mech. 29, 226–242.

Patel, B.P., Ganapati, M., Makhecha, D.P., 2002. Hydrothermal effects on the structural behavior of thick composite laminates using higher order theory. Compos. Struct. 56, 25–34.

Reddy, J.N., 1997. Mechanics of Laminated Composite Plates—Theory and analysis. CRC Press, Boca Raton, FL.

Reddy, J.N., Hsu, Y.S., 1980. Effects of shear deformation and anisotropy on the thermal bending of layered composite plates. J. Thermal Stresses 3, 475–493.

Rohwer, K., Rolfes, R., Sparr, H., 2001. Higher order theories for thermal stresses in layered plates. Int. J. Solids Struct. 38, 3673–3687.

Rolfes, R., Noor, A.K., Sparr, H., 1998. Evaluation of transverse thermal stresses in composite plates based on first order shear deformation theory. Comput. Meth. Appl. Mech. Eng. 167, 355–368.

Stavsky, V.I., 1963. Thermoelasticity of heterogeneous and aelotropic plates. J. Eng. Mech. ASCE 89, 89–105.

Tauchert, T.R., 1991. Thermally induced flexure, buckling and vibration of plates. Appl. Mech. Rev. 44, 347–360.

Tungikar, V.B., Rao, K.M., 1994. Three-dimensional exact solution of thermal stresses in rectangular composite laminate. Compos. Struct. 27, 419–430.

Whitney, J.M., 1973. Shear correction factors for orthotropic laminates under static load. Trans. ASME: J. Appl. Mech. 40, 302–304.

Wu, C.H., Tauchert, T.R., 1980a. Thermoelastic analysis of laminated plate. Part I: Symmetric specially orthotropic laminates. J. Thermal Stresses 3, 247–259.

Wu, C.H., Tauchert, T.R., 1980b. Thermoelastic analysis of laminated plate. Part II: Antisymmetric cross-ply and angle-ply laminates. J. Thermal Stresses 3, 365–378.

Xioping, S., Liangxin, S., 1994. Thermo-mechanical buckling of laminated composite plates with higher order transverse shear deformation. Comput. Struct. 53, 1–7.

Xu, K., Noor, A.K., Tang, Y.Y., 1995. Three-dimensional solutions for coupled thermo-electro-elastic response of multilayered plates. Comput. Meth. Appl. Mech. Eng. 126, 355–371.